# Novel stacked folded cores for blast-resistant sandwich beams

M. Schenk, S.D. Guest, G.J. McShane *

University of Cambridge, Department of Engineering, Trumpington Street, Cambridge CB2 1PZ, UK

A B S T R A C T

Recent research has established the effectiveness of sandwich structures with metallic cellular cores for blast mitigation. The choice of core architecture can enhance sandwich performance, dissipating energy through plastic core compression and exploiting fluid–structure interaction effects to reduce the momentum imparted to the structure by the blast. In this paper we describe the first analysis of a novel sandwich core concept for blast mitigation: the stacked folded core. The core consists of an alternating stacked sequence of folded sheets in the *Miura* (double-corrugated) pattern, with the stack oriented such that the folding kinematics define the out-of plane compressive strength of the core. It offers a number of distinct characteristics compared to existing cellular cores. (i) The kinematics of collapse of the core by a distinctive folding mechanism give it unique mechanical properties, including strong anisotropy. (ii) The fold pattern and stacking arrangement is extremely versatile, offering exceptional freedom to tailor the mechanical properties of the core. This includes freedom to grade the core properties through progressive changes in the fold pattern. (iii) Continuous manufacturing processes have been established for the *Miura* folded sheets which make up the core. The design is therefore potentially more straightforward and economical to manufacture than other metallic cellular materials. In this first investigation of the stacked folded core, finite element analysis is used to investigate its characteristics under both quasi-static and dynamic loading. A dynamic analysis of an impulsively loaded sandwich beam with a stacked folded core reveals the versatility of the concept for blast mitigation. By altering the fold pattern alone, the durations of key phases of the dynamic sandwich response (core compression, beam bending) can be controlled. By altering both fold pattern and sheet thickness in the core, the same is achieved without altering the density of the core or the mass distribution of the sandwich beam.

© 2014 Elsevier Ltd. All rights reserved.

## 1. Introduction

The response of metallic sandwich structures with cellular cores has been extensively investigated for blast mitigation applications. It has been established that a sandwich structure can outperform an equal mass monolithic plate. Key contributions to sandwich performance include the dissipation of energy through dynamic core compression, and the exploitation of fluid–structure interaction effects to reduce the momentum imparted by a blast (Xue and Hutchinson, 2004; Fleck and Deshpande, 2004; McShane et al., 2007). A wide range of metallic cellular cores have been investigated for this purpose, including: metallic foams (Deshpande and Fleck, 2000; Radford et al., 2006), periodic arrays of bars such as the pyramidal and tetrahedral lattices (Sypeck and Wadley, 2001; Kooistra et al., 2004) and prismatic cores such as the hexagonal honeycomb, square honeycomb and corrugated core (Côté et al., 2004; Côté et al., 2006; Doyoyo and Mohr, 2003;

Mohr and Doyoyo, 2004). The dynamic compressive collapse of the cellular core plays an important role in the sandwich response to blast loading (Vaughn and Hutchinson, 2006; Radford et al., 2007; McShane et al., 2012).

In this paper we describe the first analysis of a novel sandwich core suitable for blast mitigation: the *Stacked Folded Core*. The concept is sketched in Fig. 1: individual folded sheets are stacked in alternating layers to form the folded core material. In Fig. 1, the folded sheets lie in the *xy*-plane, with alternating layers stacked in the *z*-direction. A key feature of the proposed concept is the fold pattern of these sheets, the *Miura-ori* (Miura, 2006); by varying the pattern, a rich variety of geometries can be achieved (Khaliulin, 2005). The core geometry is described in Section 2 of this paper, with further details in Schenk and Guest (2013). The stacked folded core offers a number of distinct characteristics compared to alternative sandwich core materials. (i) There is exceptional versatility in the core geometry (via the fold pattern and stacking) to alter the collapse kinematics and hence mechanical properties. (ii) The fold pattern can be continuously varied through the thickness of the sandwich core (while preserving the fold kinematics), permitting

* Corresponding author. Tel.: +44 (0)1223 332635.
  *E-mail address:* gjm31@cam.ac.uk (G.J. McShane).
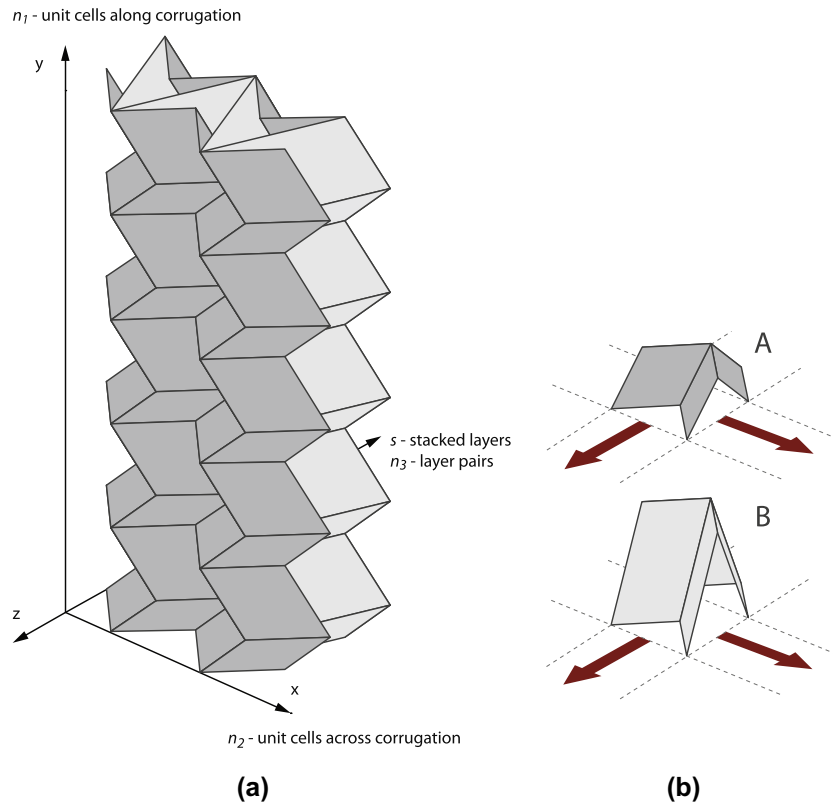
**Fig. 1.** (a) The geometry of the stacked folded core concept. The folded layers are stacked in the *z*-direction, forming a cellular material defined by: $n_1$ unit cells along the corrugation, $n_2$ unit cells across the corrugation, and *s* stacked layers with $n_3$ repeating layer pairs. The proposed sandwich core material is oriented with its *y*-axis parallel to the out-of-plane axis of the sandwich panel. (b) Examples of repeating unit cells from adjacent layers of the stack, referred to as layers *A* and *B*. The arrows lie in the *x–y* plane, and indicate the direction of tessellation of the unit cells that make up the folded sheet.

graded core properties. (iii) There are established continuous manufacturing processes for the *Miura* folded sheet comprising the core layers. (iv) The core folding kinematics are amenable to application in active or deployable structures. In the following we briefly outline the background to the core development.

### 1.1. Folded cores

An early example of a sandwich core employing the *Miura-ori* pattern was reported by Rapp (1960), and consists of a single folded layer between two facesheets. Miura (1972) derived expressions for the mechanical properties of the core, and listed among its advantages a high shear modulus and strength, an isotropic or controllable shear modulus, and improved buckling resistance due to the ruled surface along the facets. Lebée and Sab (2010) derived analytical and numerical upper and lower bounds for the shear stiffness of chevron folded core materials in a sandwich panel configuration. There have been a number of experimental and numerical investigations of the large deformation compressive collapse of folded cores, including impact energy absorption (refer to Heimbs et al. (2010) for an overview). It is noted that the buckling of the facets of the folded core play an important role in the out-of-plane compression of the folded sheet. A range of methods to introduce appropriate imperfections to finite element models in order to correctly predict this buckling is discussed by Heimbs (2009) and Baranger et al. (2011). We note, however, that the proposed stacked folded core is less imperfection sensitive, as the collapse mode does not rely on buckling of the facets, but rather the folding kinematics of the folded layers.

### 1.2. Multi-layer folded cores

An important feature of the proposed concept is the use of multiple layers of folded sheets to create the sandwich core material. Basily and Elsayed (2004) investigated the energy absorbing properties of multi-layered core structures, where folded layers were separated by flat sheets. The folded layers and flat sheets were bonded, to inhibit the unfolding of the cores upon impact. The energy absorption of the core material was investigated for different loading directions, and was found to be equivalent to or outperform similar honeycomb structures. Kling (2010) proposed several methods for stacking and joining the folded layers into multi-layered structures. These include stacking multiple layers of identical folded sheets, or alternating sequences of folded sheets with flat or singly-corrugated sheets. Kling (2010) also recognises that the overall folding kinematics can be preserved when stacking identical folded sheets, creating a customisable cellular material with tailored mechanical anisotropy. In that case, the folded sheets are joined along the fold lines, either by providing a slight offset to glue facets to facets, or creating a local inversion along the ridges to slot the next layer into.

The approach taken in this paper has two key novelties compared to existing folded core materials. (i) In the stacking of folded *Miura* layers, the fold pattern is varied alternately. This allows for a simpler method of bonding the layers whereby each layer simply slots within the fold lines of the previous one. (ii) In using the material as a sandwich core, the stacked layers are oriented so that the folding kinematics of each layer governs the out-of-plane compressive strength and stiffness of the core (the *y*-direction in Fig. 1). Previous research (Tilbrook et al., 2006; Liang et al., 2007; McShane

et al., 2007) indicates that the ability to tailor out-of-plane compressive characteristics is particularly important for optimising sandwich structures for blast mitigation.

### 1.3. Manufacture of multi-layer folded cores

Manufacturing the stacked folded core reduces to two separate problems: the manufacture of folded sheets, and the joining of these sheets in the stack. Here we briefly review techniques for manufacturing the folded *Miura* sheet (refer to Schenk (2011) for a more detailed overview). These specialised techniques aim to overcome two key challenges associated with the manufacture of folded sheets. Firstly, due to the fold line geometry, there is strong coupling between adjacent folds. This means it is difficult to simultaneously have both folded and unfolded regions in the sheet material. Secondly, during the folding process the sheets contract significantly in-plane, whilst expanding in thickness. Existing methods that solve these problems are categorised as follows.

#### 1.3.1. Synchronous methods

In synchronous folding methods, folding takes place along all fold lines simultaneously. The process often employs a mandrel consisting of hinged rigid plates which fold with the sheet (Khaliulin and Dvoeglazov, 2001; Akishev et al., 2009). The synchronous methods involve the least amount of deformation of the sheet material, reducing distortion of the folded sheet. However, it is a batch process, and the mandrel limits the practical size of the final folded sheets, making this approach more suited to prototype manufacture. In Appendix A we present a synchronous folding method suitable for producing metallic *Miura* folded sheets for laboratory-scale investigations of the stacked folded core.

#### 1.3.2. Gradual folding methods

In recent years there has been renewed interest in folded core materials for lightweight sandwich panels for aircraft construction (Heimbs et al., 2010; Baranger et al., 2011), which has also spurred the development of continuous manufacturing techniques for these folded sheets. In the gradual folding processes, the sheet material undergoes a gradual transition from flat to the fully folded state, requiring (minimal) bending of the facets between the fold lines. The gradual folding can be achieved by progressive folding through a series of mating patterned rollers (Kling, 2007). Alternatively, the desired folding pattern is embossed onto the flat sheet material, creating a residual stress field which initiates the folding process; progressive folding then takes place by tapered guides contracting the sheet to its desired width (Kehrle, 2005). As a continuous process, the gradual folding method has the advantage of increased output rates compared to batch processes. Limitations include costly tooling (*e.g.* for patterned rollers), and limits on the sheet material rigidity (for the patterning and gathering method).

#### 1.3.3. Pre-gathering methods

Another approach aims to overcome the coupled longitudinal and transverse contraction, by first pre-gathering the sheet material into a singly corrugated sheet. The double corrugation can then be created row-by-row. For example, the double corrugation can be created by periodically inverting the single corrugations (Hochfeld, 1959), or moving the straight corrugations alternately sideways (Khaliulin et al., 2007). The second phase can also be achieved continuously, by passing the corrugated material through a set of mating patterned rollers that impart the final shape (Ichikawa, 1995; Elsayed and Basily, 2004). The pre-gathering methods involve significant material deformations and require expensive dedicated tooling, but are relatively versatile, permitting a wide range of fold patterns and sheet materials.

### 1.4. Outline of the paper

The objectives of this investigation are twofold: (i) To describe the geometric parameters for the stacked folded core concept, and hence illustrate the versatility of this novel cellular material. (ii) To use finite element analysis to assess the quasi-static and blast response of the stacked folded core, as part of a sandwich beam structure, as the fold pattern is adjusted over a wide range. The paper is structured as follows. In Section 2, the unit cell and stacked folded core geometries are defined, and the fold parameters linked to the folding kinematics and core density. In Section 3, finite element analysis is used to investigate the quasi-static compressive collapse of the core. The influence of unit cell parameters and boundary conditions are considered. In Section 4, dynamic finite element calculations are reported, demonstrating the response of a sandwich beam with a stacked folded core to impulsive loading. The influence of the core fold parameters on the dynamic response are evaluated. Conclusions are provided in Section 5.

## 2. Geometry of the stacked folded core

An important feature of the stacked folded core is its versatile geometry. By varying the fold pattern and the stacking sequence, the mechanical properties of the core material can be tailored. In this section the core geometry and kinematics are described, and the rich geometric design space is highlighted.

### 2.1. Unit cell geometry

The *Miura-ori* folded layers in the stacked folded core consist of a tesselation of unit cells, as shown in Fig. 2(a) (Miura, 2006). The unit cell geometry can be described in various ways; the parameterisation used here is by the dimensions of its folded configuration, with height $H$, width $2S$, length $2L$ and amplitude $V$. These can be converted to the dimensions of the required fold pattern on the flat sheet, Fig. 2(b), as follows:

$$L_0 = \sqrt{H^2 + L^2} \tag{1}$$

$$S_0 = \sqrt{\frac{H^2 V^2}{H^2 + L^2} + S^2} \tag{2}$$

$$V_0 = \frac{LV}{\sqrt{H^2 + L^2}}. \tag{3}$$

The thickness $t$ of the sheet material folded to form the cell completes the description.

### 2.2. Layer stacking

The *Miura-ori* folded layers are stacked to form a sandwich core as shown in Fig. 1. Successive layers nest within each other along common fold lines. To allow this nesting, successive layers share the same $S$, $L$ and $V$, leaving the heights of the layers, $H$, to be chosen independently. $H$ could be varied arbitrarily from layer to layer. However, we shall here focus on an *ABABA* stacking configuration, where the fold pattern alternates between layers, with $H_B \geqslant H_A$. The result of this stacking process is a cellular folded meta-material that is highly anisotropic in its mechanical properties. The arrangement of the stack for a complete sandwich core is illustrated in Fig. 3. The in-plane dimensions are $L_c$ and $W_c$, denoting the length and width of the sandwich beam core. The out-of-plane dimension (the core depth) is $D_c$. The beam dimensions $D_c$, $L_c$ and $W_c$ are determined by the dimensions of the unit cells $(S, L, H_A, H_B)$ and the number of repeating unit cells $(n_1, n_2, n_3)$. There are $n_1$ unit cells along the corrugation, $n_2$ unit cells across
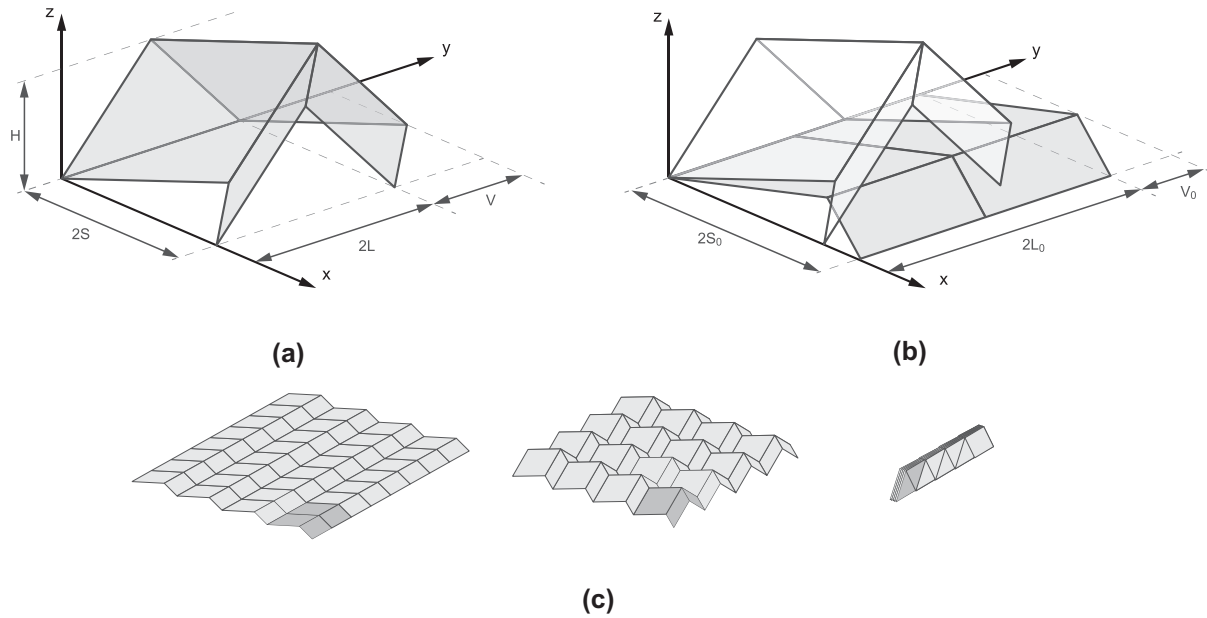
**Fig. 2.** (a) The dimensions of the *Miura-ori* unit cell. (b) The fold line dimensions on the flat sheet. (c) A folded sheet shown in three stages of its folding process, from a flat sheet to fully folded.
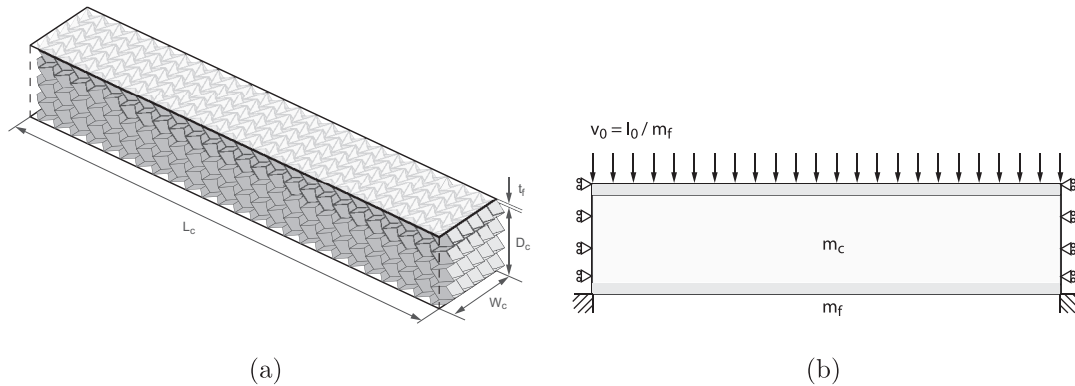


**Fig. 3.** (a) Orientation of the stacked folded core in a sandwich beam configuration. The overall core dimensions are given by the length $L_c$, width $W_c$, and height $D_c$. The folded *Miura* layers are stacked across the width of the beam, as shown in Fig. 1(a). The facesheets have thickness $t_f$. (b) The applied loading and boundary conditions for the dynamic analysis (see Section 4). The blast loading is simulated by imposing an initial velocity $v_0 = I_0/m_f$ to the front face sheet, with $m_f$ the face sheet mass and $I_0$ the total impulse. The mass of the core is $m_c$.

the corrugation, and $s$ layers in the stack, with $n_3$ repeating layer pairs $AB$; see Fig. 1. The core dimensions are then given by:

$$D_c = n_1 \cdot 2S \tag{4}$$

$$L_c = n_2 \cdot 2L \tag{5}$$

$$W_c = n_3 \cdot (H_B - H_A) + H_A. \tag{6}$$

### 2.3. Core relative density

For a single folded sheet, expressions for the relative density $\bar{\rho} = \rho_c/\rho$ (where $\rho_c$ is the core density and $\rho$ the density of the sheet material from which it is fabricated) have previously been derived (Klett and Drechsler, 2010; Schenk and Guest, 2013). For the *ABABA* stacked folded core configuration, the core relative density can be described in terms of the fold parameters and sheet thickness $t$, as follows:

$$\bar{\rho} = \frac{t/L}{H_B/H_A - 1} \cdot \left[ \sqrt{1 + \left(\frac{L}{H_A}\right)^2 + \left(\frac{V}{S}\right)^2} + \frac{H_B}{H_A} \sqrt{1 + \left(\frac{L}{H_B}\right)^2 + \left(\frac{V}{S}\right)^2} \right]. \tag{7}$$

We note that the core density can be controlled by adjusting any one of four independent non-dimensional groups: $t/L, H_B/H_A, L/H_A$, and $V/S$. This provides considerable freedom for design and optimisation, allowing a wide range of fold patterns (and hence mechanical properties) to be obtained for a fixed value of core relative density $\bar{\rho}$.

### 2.4. Folding kinematics

The out-of-plane compressive response of the stacked folded core material is dominated by the kinematics of the fold pattern. Assuming that each of the facets remains rigid and the fold lines behave like hinges, and neglecting for the moment the constraint provided by any face sheets in a sandwich structure (this will be described subsequently), a folded *Miura-ori* layer has a single planar mechanism, characterised by its kinematic expansion coefficient (Schenk and Guest, 2013):

$$v_{SL} = -\frac{\varepsilon_L}{\varepsilon_S} = -\frac{S}{L} \frac{dL}{dS} = -\left(\frac{S}{V}\right)^2 \tag{8}$$

Here $\varepsilon_L$ and $\varepsilon_S$ represent nominal strains in the *x*- and *y*-directions of the unit cell, respectively (Fig. 2). The kinematics of each folded sheet are thus only determined by the in-plane dimensions *S* and *V*. Furthermore, $v_{SL}$ is always negative. Notably, the folding kinematics do not depend on the height $H_A$ and $H_B$ of the folded layers. Therefore, when stacking the sheets, the expansion coefficient will be constant across all layers, and the folding kinematics are preserved. This realisation is also used to advantage in manufacturing of folded sheets (Khaliulin and Dvoeglazov, 2001). The coupling between folding of the *Miura-ori* layers and the change in width $W_c$ of the stacked configuration is also described by an expansion coefficient. For large values of $n_3$ this is shown to be always negative by Schenk and Guest (2013), and the stacked folded core material therefore has a negative Poisson's ratio in all directions. Further discussion of materials that display a negative Poisson's ratio (auxetics) can be found in Lakes (1987).

The densification (lock-up) strain of the stacked folded core – the point at which the *Miura-ori* layers are fully collapsed – also depends on the core geometry. When the core is fully collapsed, the amount of overlap between successive *A* layers (which will affect the densification strain) depends on the height $H_B$ of the intermediate *B* layers. Furthermore, it has been shown that the geometry of the unit cells can be varied within each of the folded layers without inhibiting its folding kinematics in the stacked configuration (Schenk and Guest, 2013). This grading of the fold pattern allows control of the timing of contact between adjoining unit cells, and hence the lock-up behaviour of the core. This may be used to optimise a core geometry, but will not be pursued further in the current work.

## 3. Quasi-static analysis of stacked folded core

The quasi-static out-of-plane compression of the stacked folded core is investigated in order to gain insight into its stiffness and strength, and the sensitivity to boundary conditions. To this end, we investigate the compression of free-standing cores of various dimensions. Finite Element Analysis, employing the commercial package ABAQUS/Standard, is used to investigate the core response.

### 3.1. Finite element model description

#### 3.1.1. Folded core geometry
In this investigation we restrict attention to the influence of varying three core parameters: the fold parameter $V/S$, the core depth $D_c$ and core length $L_c$ (respectively $n_1$ and $n_2$ unit cells). The range of values considered for these variables will be defined subsequently. The dimensionless ratio $V/S$ controls the 'chevron' angle of the fold pattern: increasing $V/S$ alters the fold pattern from a simple corrugation at $V/S = 0$ to a double corrugation, or 'chevron', pattern at larger values; see Fig. 4. The other fold parameters used in this analysis are held constant, with $S = L = H_A = 0.010$ m and $H_B = 0.025$ m. In all cases a sheet thickness of $t = 0.173$ mm (37 SWG) and a core width of $s = 5$ ($n_3 = 2$) layers was used.

#### 3.1.2. Boundary conditions
The boundary conditions are defined in the *xyz*-coordinate system shown in Fig. 1. For the bottom edges of the core (the edges at $y = 0$), all degrees of freedom are constrained to be zero. For the top edges of the core (at $y = D_c$), a vertical displacement $\delta$ in the negative *y*-direction is prescribed, with all other degrees of freedom set to zero. These boundary conditions represent the displacement controlled compression of the core between rigid face
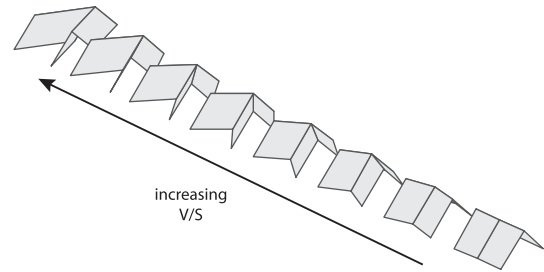


**Fig. 4.** The folded sheet can range from a single to double corrugation by varying the dimensionless parameter $V/S$. Here is shown a range of $V/S = 0$–2, with fixed $H = S = L$.

sheets, to which it is perfectly bonded. The nominal core compression is defined as:

$$\bar{\varepsilon} = \frac{\delta}{D_c}.\tag{9}$$

All other free edges in the core stack are left unconstrained. No element contact constraints were specified in the quasi-static analysis, and hence calculations were stopped before element contact was observed.

#### 3.1.3. Finite element discretisation
The folded sheets were meshed with linear shell elements with reduced integration, hourglass control and finite membrane strains (element type *S4R* in ABAQUS notation). Along the fold lines of individual sheets, common nodes of adjoining facet edges are tied (*i.e.* all degrees of freedom are fixed to be identical). Hence no relative rotation of adjacent facet edges is permitted, with folding taking place by elasto-plastic facet bending adjacent to the hinge line. Similarly, adjacent layers in the stack of folded sheets were connected by tying degrees of freedom at the contacting fold lines. In practice, hinge behaviour in metallic folded *Miura* sheets is likely to be more complex, with details of the manufacturing process having an influence. This includes residual stresses from folding the sheets, as well as the method of bonding the sheets into the stacked configuration (*e.g.* brazing, gluing). However, investigation of these detailed hinge effects is beyond the scope of the current study. Each facet of the *Miura* sheet was meshed with $22 \times 22$ elements, with a local refinement near the fold lines to capture the bending deformations. A mesh convergence study showed that the core response is insensitive to further mesh refinement.

#### 3.1.4. Material model
An elastic–plastic material model representative of High Strength Low Alloy steel HSLA-65 was selected for the folded sheet material. This steel was selected as a material suited to high performance structural applications which has also been characterised at a wide range of strain rates (Nemat-Nasser and Guo, 2005). The material density is 7800 kg m$^{-3}$. Linear elastic behaviour with Young's modulus $E = 200$ GPa and Poisson's ratio $v = 0.3$ was specified. Plastic behaviour follows $J_2$ flow theory with isotropic hardening. Strain and strain-rate dependent hardening are specified using the Johnson–Cook model (Johnson and Cook, 1983), as follows:

$$\sigma_y = (A + B\hat{\varepsilon}^n) \cdot \left[1 + C\ln\left(\frac{\dot{\hat{\varepsilon}}}{\dot{\varepsilon}_0}\right)\right]\tag{10}$$

where $\sigma_y$ is the yield stress, $\hat{\varepsilon}$ is the effective plastic strain, and $A, B, n, C$ and $\dot{\varepsilon}_0$ are material parameters. Temperature dependent plasticity and material damage have not been included in our

(a)



(b)
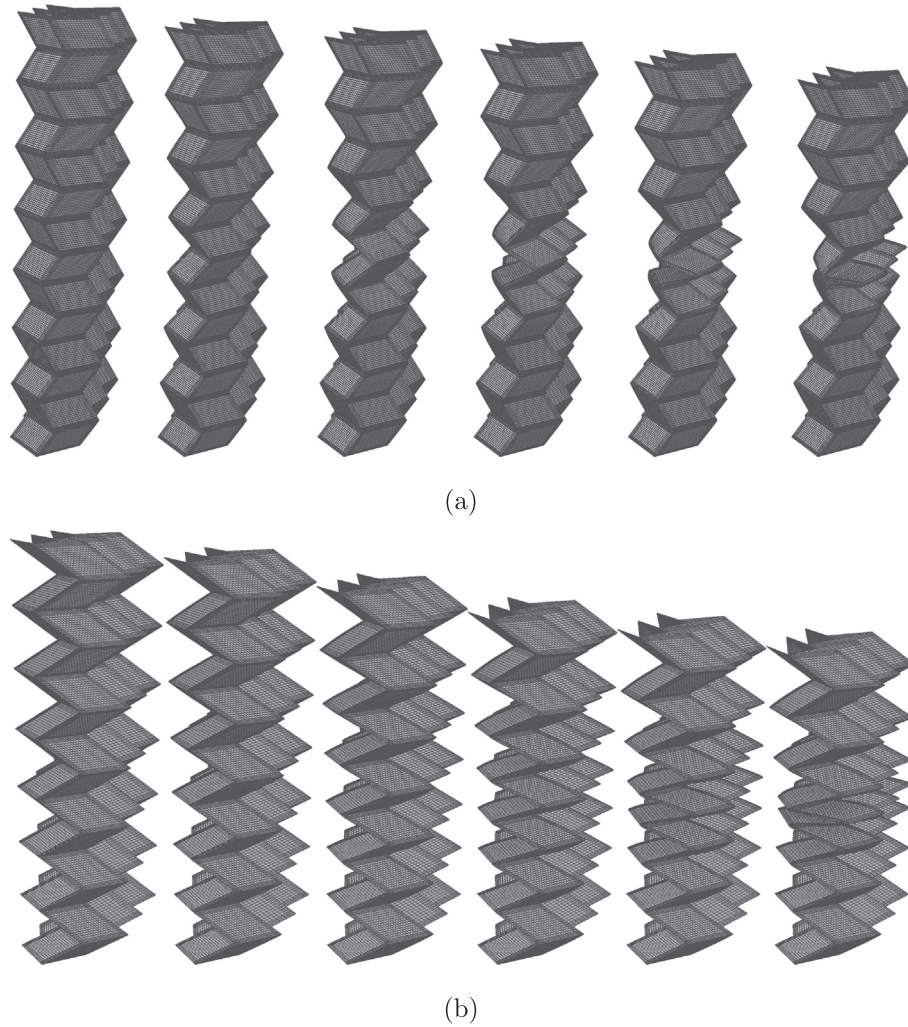
**Fig. 5.** Deformation under compression of a single column with $n_1 = 7$ unit cells. Shown are deformed configurations, from the undeformed state to the point of first observed contact, for (a) $V/S = 0.5$ and (b) $V/S = 1.25$.

current analysis.[1] The Johnson–Cook parameters for HSLA-65 steel have been measured by Nemat-Nasser and Guo (2005). The parameters used in the current investigation, derived from the data of Nemat-Nasser and Guo (2005) at a temperature of 296 K, are as follows: $A = 390$ MPa, $B = 625$ MPa, $n = 0.25, C = 0.022$ and $\dot{\varepsilon}_0 = 1$ s$^{-1}$.

### 3.2. Single column response

The compressive response of a single column of stacked cells ($n_2 = 1$) is first studied for two scenarios: (i) a constant core depth ($n_1 = 7$) with variable ratio $V/S = 0.25-2$; (ii) a varying core depth, $n_1 = 3-7$, with a constant $V/S = 0.5$.

*Case (i):* Illustrations of the deformed configuration at different levels of core compression $\bar{\varepsilon}$ are shown in Fig. 5 for two values of $V/S$. The vertical force required to compress the core is plotted in Fig. 6(a) against the nominal core compression for a range of $V/S$. To allow comparison with results for larger stacks, the reaction

force $F$ is given normalised by the number of cells along the length and width of the stack:

$$F = \frac{F_t}{n_2 \cdot n_3} \tag{11}$$

where $F_t$ is the total reaction force required to compress the core. The reaction force $F$ is further normalized as follows:

$$\bar{F} = \frac{F}{\bar{\rho}\sigma_y A} \tag{12}$$

where the projected area of a single column of cells $A = 2L(H_B - H_A)$, the core relative density $\bar{\rho}$ (for $V/S = 0.50$, $\bar{\rho} = 0.052$) and the sheet material yield strength $\sigma_y = 390$ MPa. This normalisation allows comparison with alternative cellular core topologies. Following the analysis of Gibson and Ashby (1999), for the bending dominated plastic collapse of a regular honeycomb $\bar{F} = 26 \times 10^{-3}$, and for an open celled foam $\bar{F} \approx 68 \times 10^{-3}$, both evaluated for $\bar{\rho} = 0.052$. The stacked folded core therefore has a comparable compressive strength to other bending dominated cellular structures.

For $V/S \lesssim 1$, Fig. 5(a), the column initially deforms uniformly, with the reaction force increasing with core compression. Plastic hinges are observed to develop along the fold lines very early in the deformation. The peak in the reaction force corresponds to

---

[1] We acknowledge that plastic deformation along the hinge lines is likely to be large, and therefore the material will be susceptible to damage and thermal softening in practice. This would in turn influence the compressive strength of the cellular material. However, we opt to omit these details in this first investigation, preferring a simple constitutive model to assist with an initial interpretation of the collapse behaviour.
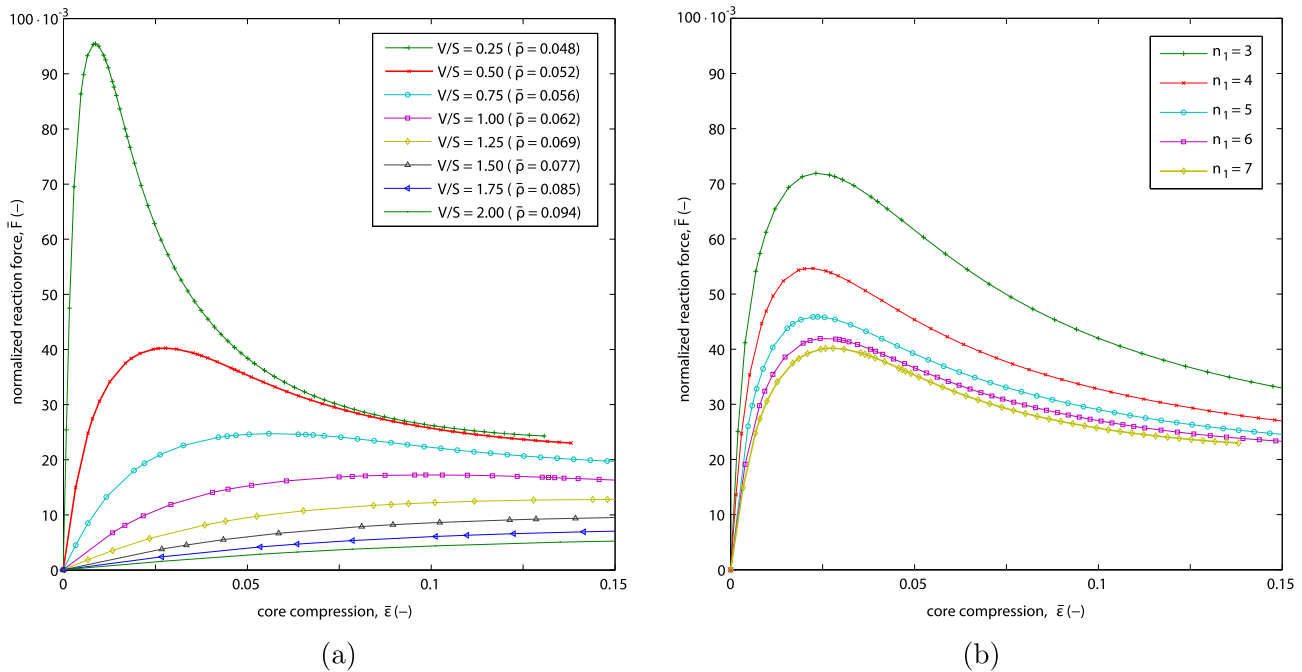
**Fig. 6.** Force-compression results for (a) a single column stack of constant height $n_1 = 7$ with varying $V/S = 0.25-2$, and (b) a single column stack with varying height, $n_1 = 3-7$, with $V/S = 0.5$.

the onset of localisation, with deformation becoming concentrated in the middle (least constrained) cell. This collapse instability initiates core softening. With increasing $V/S$ the column becomes progressively softer, with lower peak reaction forces. Furthermore, for $V/S \gtrsim 1$, localisation does not appear to take place, with the deformation remaining relatively uniform throughout the height of the column, Fig. 5(b). For values of $V/S \gtrsim 1$, strong softening of the core no longer occurs, with the reaction force rising to a plateau of approximately constant force.

*Case (ii):* To assess the influence of core depth on the localisation phenomena observed for $V/S \lesssim 1$ we consider next the influence of altering $n_1$ with $V/S = 0.5$. The force required to compress the core for this case is plotted in Fig. 6(b). The core strength during the early phase of compression and the peak reaction force attained (at the onset of localisation) are both greater for shorter columns (smaller $n_1$). This can be attributed to the greater influence of the boundary constraints (representing the face sheets) on the kinematics of core collapse. The peak reaction force converges as the stack height is increased, as these boundary effects cease to influence the localised deformation in the centre of the column.

### 3.3. Multi-column response

Next is considered the influence of the number of unit cells $n_2$ along the length of the sandwich core, with the core depth fixed at $n_1 = 7$. Again, two scenarios are studied: (i) a constant core length $n_2 = 5$ with varying $V/S = 0.25-2$; and (ii) a variable core length, with $n_2 = 1-7$ with constant $V/S = 0.5$.

*Case (i):* Deformed configurations are shown in Fig. 7 for two values of $V/S$. Notable is the effect of the negative Poisson's ratio on the deformed configuration. For $V/S = 0.5$ the central row of unit cells (furthest from the facesheets) contract significantly in the transverse direction, whereas for $V/S = 1.25$ the width of the stack does not change noticeably during compression. The force required to compress the cores are plotted in Fig. 8(a), normalised as described by Eq. (11) to allow comparison with the single

column results. Similar to the single column case, increasing $V/S$ reduces the core strength. For $V/S \gtrsim 1$, there is again a lack of strong localisation, and the core deforms uniformly, without softening. The additional constraint provided by the increased number of cells in the stack results in larger peak reaction forces (per unit cell column, Eq. (11)), and more gradual softening for the larger $V/S$ cases, for a given fold pattern. The peak reaction force is also more sensitive to $V/S$ than the single column case.

*Case (ii):* The influence of this constraint effect is demonstrated further in Fig. 8(b). As the number of cells along the length of the core is increased, the core becomes significantly stronger (per unit cell column, Eq. (11)) in compression, as the influence of the free edges diminishes. It is observed that for narrow stacks (*e.g.* $n_2 = 1, 3$) the deformation is concentrated at the central unit cells, furthest from the face sheets. For wider stacks (*e.g.* $n_2 = 5, 7$) the deformation is more uniformly distributed, increasing the overall compressive strength.

## 4. Dynamic response of sandwich beams

In this section we use the commercial finite element package ABAQUS/Explicit to investigate the response of a sandwich beam with a stacked folded core to an impulsive load applied to the top face sheet. We investigate the influence of core fold parameters on the sandwich response, considering performance metrics such as back face sheet deflections and support reactions.

### 4.1. Finite element model description

The geometry and boundary conditions of the sandwich beam are shown in Fig. 3. The beam has span $L_c = 0.5$ m, core depth $D_c = 0.08$ m and width $W_c = 0.04$ m. The face sheet thickness $t_f$ is varied, and will be defined subsequently. In this investigation $t_f$ is the same for both the front face sheet (defined as that facing the blast) and the back face sheet. The boundary conditions adopted in this investigation are similar to those employed by Tilbrook et al. (2006). The ends of the core (nominal area $W_c \cdot D_c$)
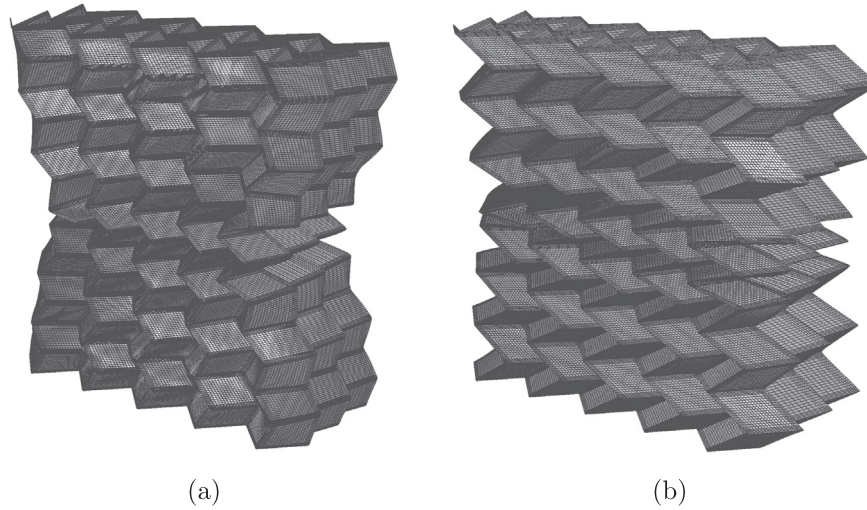
**Fig. 7.** Deformed configuration for a stack with $n_1 = 7$ and $n_2 = 5$ unit cells, for (a) $V/S = 0.5$ and (b) $V/S = 1.25$.
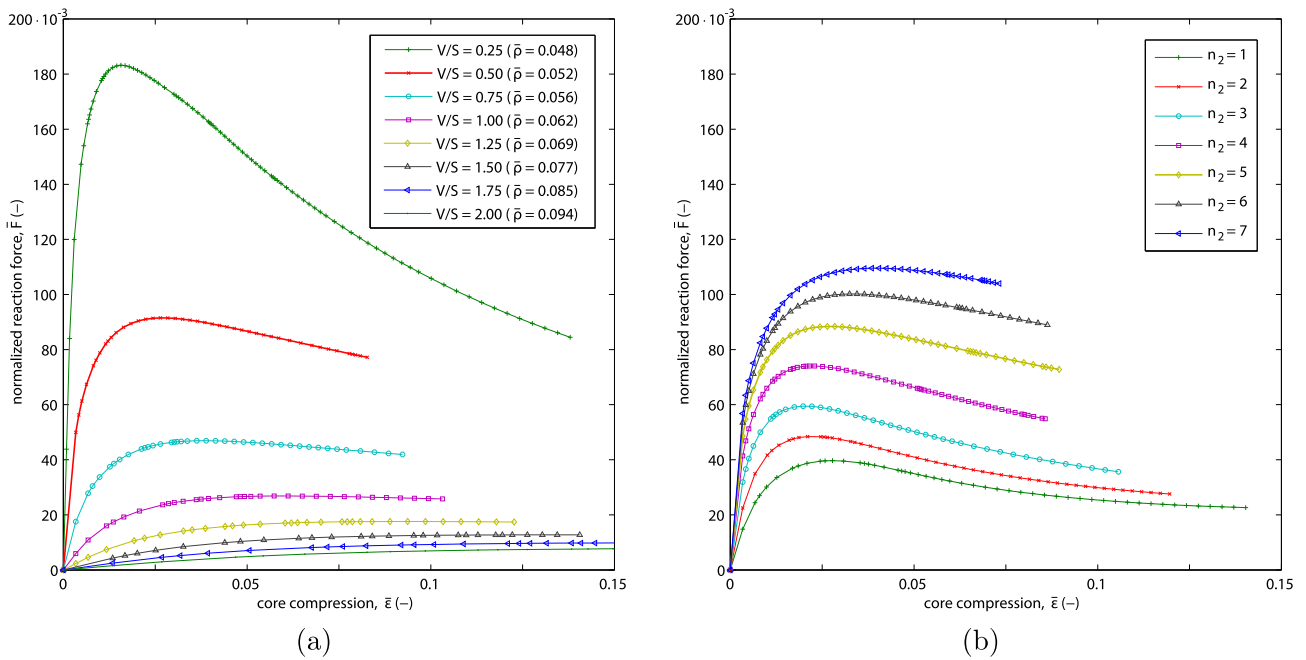


**Fig. 8.** Force-compression results for (a) a multi-column stack ($n_1 = 7$ and $n_2 = 5$) with varying $V/S$, and (b) a multi-column stack ($n_1 = 7$, $V/S = 0.50$) with varying a varying core length of $n_2 = 1–7$ unit cells.

are constrained against horizontal motion as shown in Fig. 3. This is representative of a repeating unit of a larger sandwich structure supported periodically on its rear face, where the supporting bulkheads do not extend through the thickness of the sandwich (which would be the case for fully clamped boundary conditions) (Tilbrook et al., 2006). We opt for a relatively narrow sandwich beam, rather than a wide sandwich plate, due to the computational cost of modelling the core structure. However, the sides of the core (nominal area $L_c \cdot D_c$) are left unconstrained, *i.e.* periodic boundary conditions were not applied. This was for two reasons. Firstly, as described in Section 3, the value and sign of the expansion coefficient in the *z*-direction will vary with the stack size, i.e. the width of the beam. For small stacks it will be positive – consider the behaviour of a single folded sheet – whereas for large stacks it will always be negative. This means that conventional periodic boundary conditions on the edges of the sandwich beam would

not accurately reflect the behaviour of a larger panel. Secondly, for the core configurations studied, the expansion coefficient in the *z*-direction is very small, and much less than that in the *xy*-plane (of the order of 1%). The beam response is therefore insensitive to the choice of constraint on the sides of the core, and the current model can reasonably be considered indicative of a larger sandwich panel. The finite element discretization (element type, element density) of the folded core is the same as reported previously for the quasi-static analysis. Face sheets were discretized using identical shell elements to the folded core, with a mesh density approximately matching that of the core facets. The ABAQUS 'general contact' option was used to define a hard, frictionless contact between all surfaces in the model, thus capturing core densification.

The material model used in the dynamic analysis is identical to that described in Section 3 above, and is representative of High

**Table 1**
Load Case 1, facesheet mass $m_f$, front face sheet initial velocity $v_0$ and corresponding imparted kinetic energy $U_k$, for a range of fold parameters $V/S$.

| $V/S$ | $m_f$ (kg) | $v_0$ (m/s) | $U_k$ (kJ) |
|---|---|---|---|
| 0 | 0.519 | 101 | 2.63 |
| 0.25 | 0.514 | 102 | 2.66 |
| 0.50 | 0.498 | 105 | 2.75 |
| 0.75 | 0.473 | 111 | 2.89 |
| 1.00 | 0.441 | 119 | 3.10 |
| 1.25 | 0.404 | 129 | 3.38 |
| 1.50 | 0.363 | 144 | 3.76 |
| 1.75 | 0.320 | 163 | 4.25 |
| 2.00 | 0.275 | 190 | 4.98 |

**Table 2**
Load Case 2, sheet thickness $t$ for a range of fold parameters $V/S$.
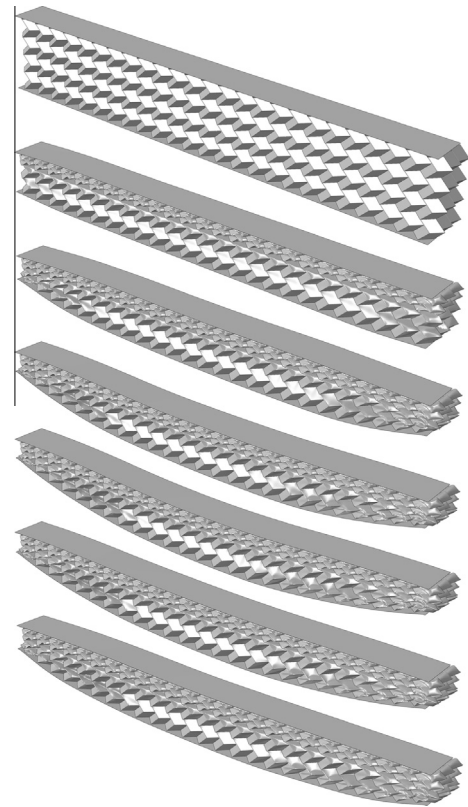
| $V/S$ | $t$ (mm) |
|---|---|
| 0 | 0.173 |
| 0.25 | 0.169 |
| 0.50 | 0.160 |
| 0.75 | 0.147 |
| 1.00 | 0.133 |
| 1.25 | 0.120 |
| 1.50 | 0.108 |
| 1.75 | 0.099 |
| 2.00 | 0.089 |
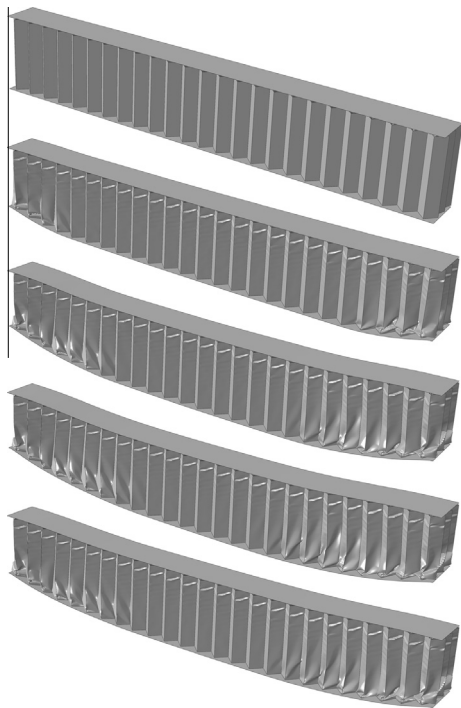


**Fig. 9.** Case 1, deformation of the beam with $V/S = 0$; snapshots taken at 0.5 ms intervals.



**Fig. 10.** Case 1, deformation of the beam with $V/S = 1$; snapshots taken at 0.5 ms intervals.
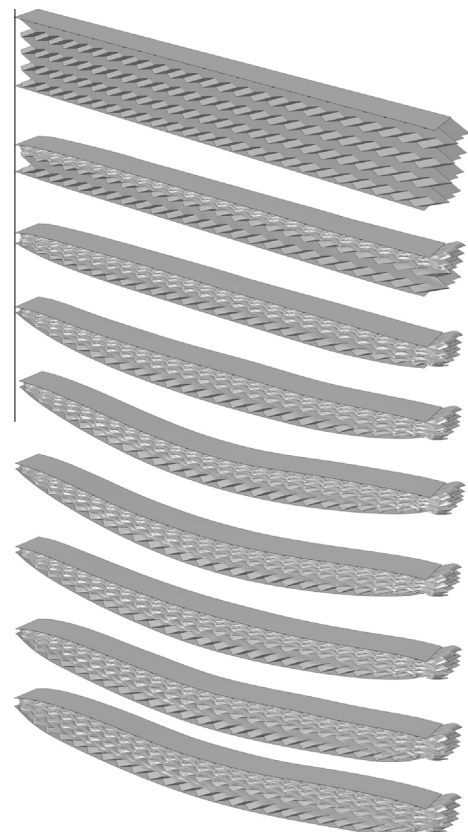


**Fig. 11.** Case 1, deformation of the beam with $V/S = 2$; snapshots taken at 0.5 ms intervals.

Strength Low Alloy steel HSLA-65. This material model is used for both the face sheets of the sandwich beam and the stacked folded core.
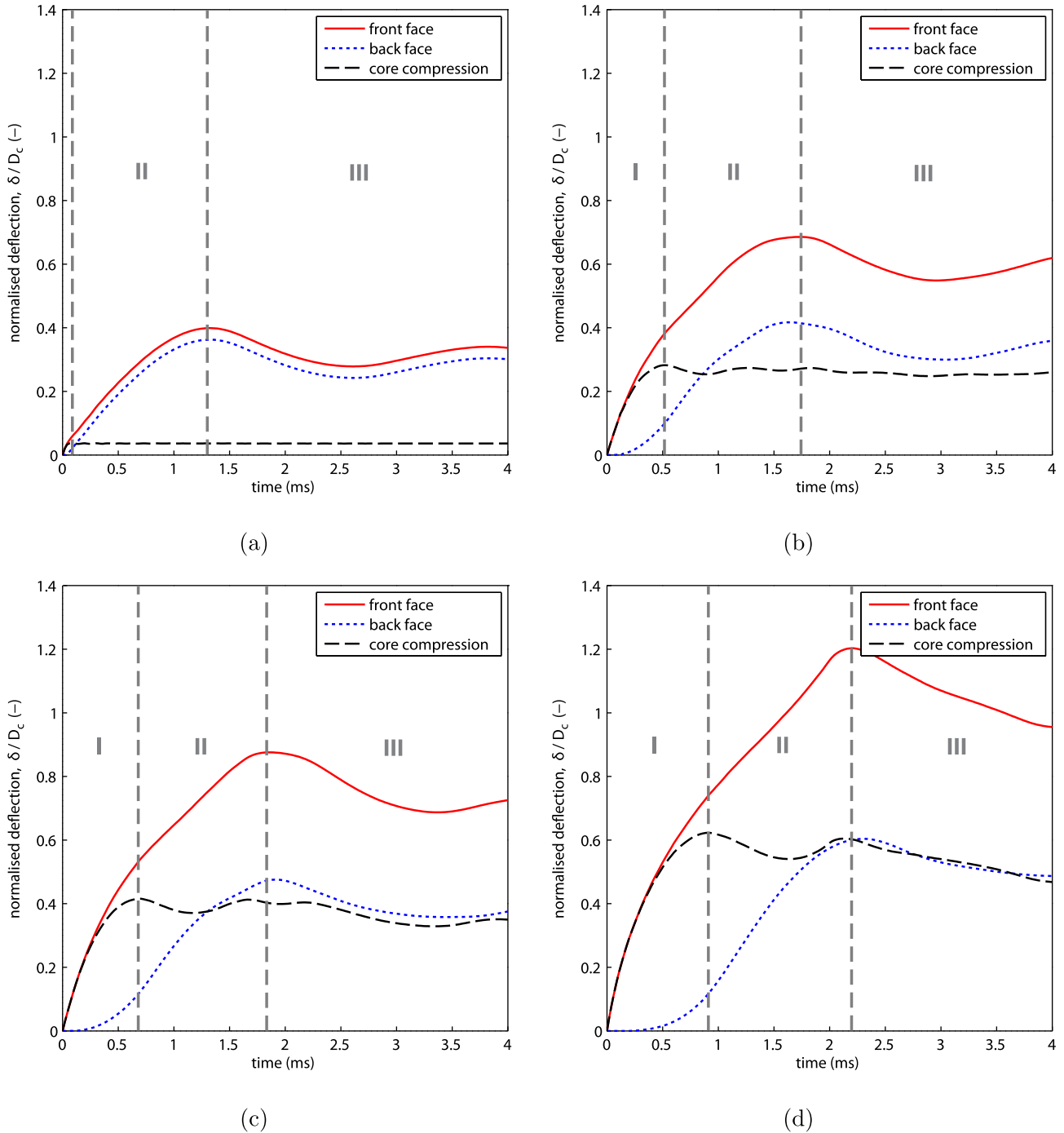
In this investigation we opt for a simplified representation of blast loading, applying an impulse $I_0 = m_f \cdot v_0$ to the front face sheet of the sandwich beam. Here $m_f$ is the front face sheet mass and $v_0$ the initial velocity applied instantaneously and uniformly

**Fig. 12.** Case 1, deflection $\delta$ at the centre of the front and back face sheets, normalised by the core depth $D_c$. The nominal core compression at mid-span, given by the difference between the normalised face sheet deflections, is also plotted. The three phases of response are indicated. (a) $V/S = 0$, (b) $V/S = 0.5$, (c) $V/S = 1$, (d) $V/S = 2$.

to the whole face sheet, as shown in Fig. 3. This approach to modelling blast loading neglects fluid–structure interaction effects which might alter the momentum imparted to the beam for different sandwich configurations (Fleck and Deshpande, 2004; Xue and Hutchinson, 2004). To allow comparison with published investigations of the blast response of sandwich beams, it is convenient to normalise the applied impulse as follows:

$$\bar{I} = \frac{I_0}{m_b} \cdot \sqrt{\frac{\rho}{\sigma_y}} \qquad (13)$$

where $\sigma_y = 390$ MPa and $\rho = 7800$ kgm$^{-3}$ are the quasi-static yield strength and density of the sheet material used for the core, respectively. The total mass of the sandwich beam $m_b = m_c + 2 \cdot m_f$, where $m_c$ is the total mass of the core, and $m_f$ is the mass of each face sheet. We restrict the scope of this investigation to a single sandwich beam total mass $m_b = 1.56$ kg, held constant in all calculations. This is equivalent in mass to a monolithic steel plate of 10 mm thickness. We also consider only a single blast impulse $\bar{I} = 0.15$, corresponding to a total impulse $I_0 = 52.3$ Ns or, expressed per unit area of plate, 2.6 kNsm$^{-2}$. This impulse magnitude is of the
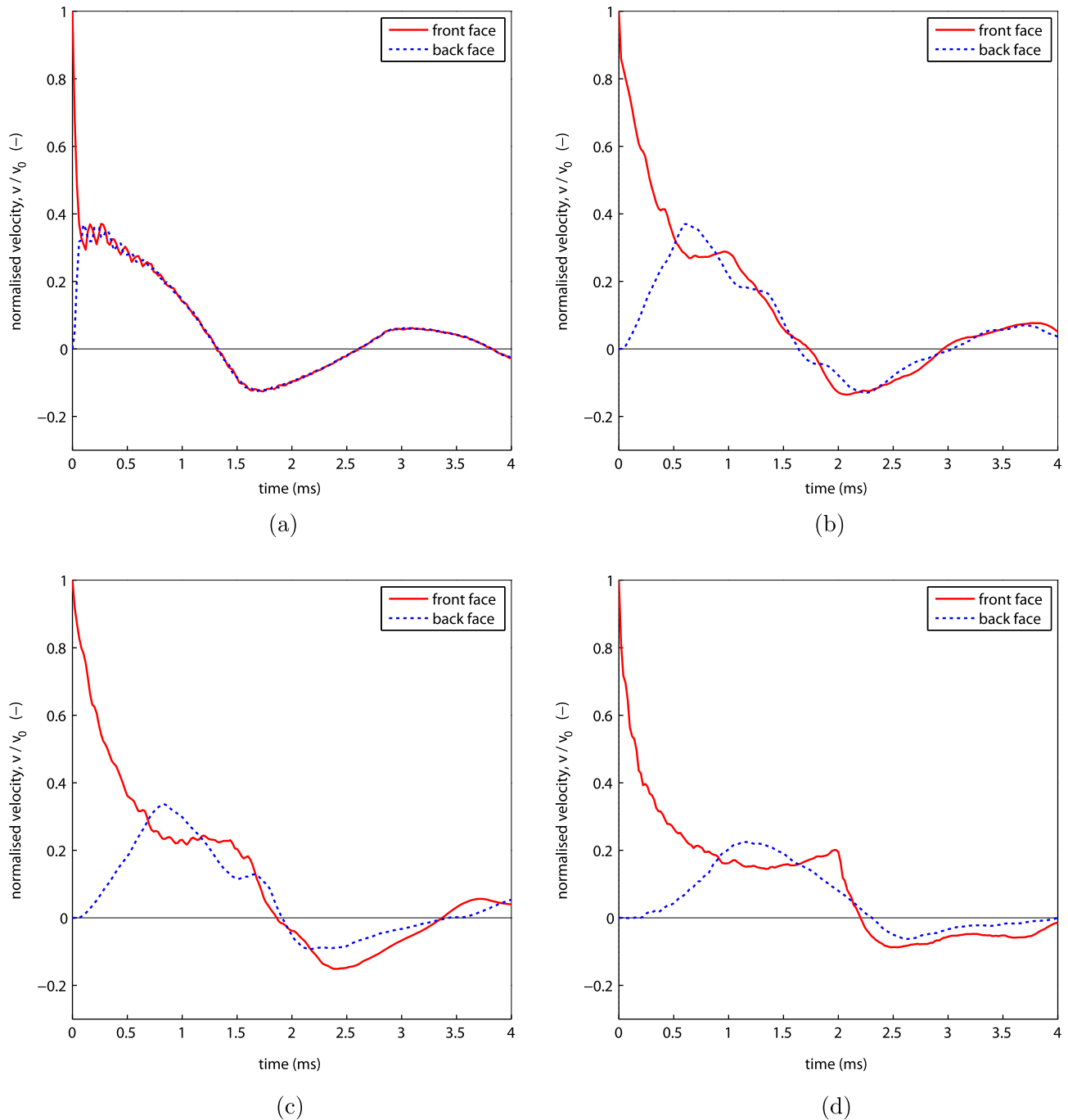
**Fig. 13.** Case 1, velocity $v$ at the centre of the front and back face sheets, normalised by the initial front face velocity $v_0$. (a) $V/S = 0$, (b) $V/S = 0.5$, (c) $V/S = 1$, (d) $V/S = 2$.

same order as that considered in a number of related studies, *e.g.* Xue and Hutchinson (2004).

### 4.2. Folded core parameters

As detailed in Section 2, the stacked folded core concept has a wide parameter space that can be exploited for blast resistance. In this investigation we again restrict attention to the influence of one fold parameter: the dimensionless ratio $V/S$ (Fig. 4). All other fold parameters are held fixed, as follows. Within the core there are $n_1 = 4$ unit cells through the core depth ($D_c$) and $n_2 = 25$ along the core length ($L_c$). There are a total of $s = 5$ layers across the width of the core ($W_c$), with $n_3 = 2$ pairs of layers $A$

and $B$ (Fig. 1). For a fixed core envelope, specifying the number of unit cells $n_1, n_2$ and $n_3$, will establish the unit cell dimensions $H, S$ and $L$ (refer to Fig. 2). The chosen sandwich core dimensions (above) lead to $S = 0.010$ m, $L = 0.010$ m, $H_A = 0.010$ m and $H_B = 0.025$ m.

One further core parameter remains free: the sheet thickness $t$. Following Eq. (7), the choice of $V$ and $t$ will determine the relative density of the core. In all calculations, the total mass of the sandwich beam will be held fixed. As parameter $V/S$ is varied, the total mass of the beam can thus be kept constant by either (i) fixing the core sheet thickness $t$ and changing the mass of the face sheets $m_f$ or (ii) fixing the mass of the face sheets $m_f$ and varying the sheet thickness $t$; both cases are considered independently.
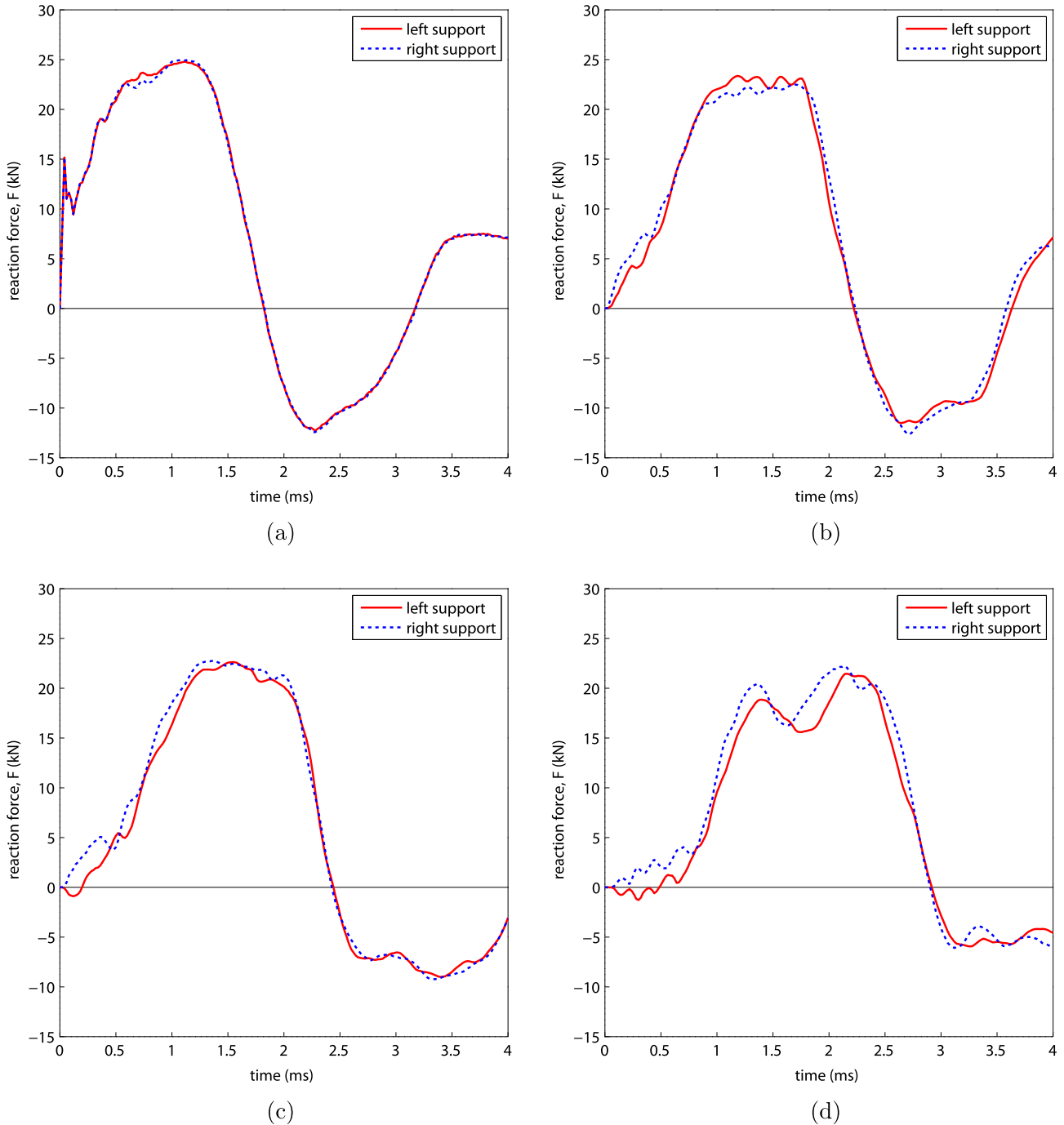
**Fig. 14.** Case 1, vertical reaction forces at the supports. (a) $V/S = 0$, (b) $V/S = 0.5$, (c) $V/S = 1$, (d) $V/S = 2$.

*Case 1: fixed core sheet thickness t.* At an arbitrary reference configuration $V/S = 0$, the mass of the face sheets and core are selected to be equal: $m_c = m_f = m_b/3 = 0.519$ kg. Each face sheet therefore has thickness $t_f = 3.3$ mm. A core sheet thickness of $t = 0.173$ mm (37 SWG) is selected to give the required total core mass for the reference configuration. This sheet thickness was used for all calculations in Case 1. As $V/S$ is increased from the reference state, the density (and therefore mass) of the core increases. The face sheet thickness $t_f$ is therefore reduced to maintain constant total sandwich mass. As the momentum imparted to the plate is held fixed, the initial velocity $v_0$ applied to the front face is therefore increased as $m_f$ is reduced. Consequently, the initial kinetic energy varies. Table 1 lists the initial velocity $v_0$ and imparted

kinetic energy $U_k$ for each core geometry studied in Case 1. (Fixing impulse, rather than kinetic energy, is a more realistic representation of a fixed blast load in the absence of fluid–structure interaction effects. Variations in kinetic energy are therefore an intrinsic consequence of the sandwich design, and do not invalidate the comparison.)

*Case 2: fixed face sheet thickness $t_f$* Again, the core sheet thickness $t = 0.173$ mm and face sheet thicknesses $t_f = 3.3$ mm are fixed in the reference core configuration $V/S = 0$ to give $m_c = m_f = m_b/3 = 0.519$ kg. Now, as fold parameter $V/S$ is increased, the core sheet thickness $t$ is reduced to maintain constant core mass. The face sheet masses $m_f$ and initial kinetic energy therefore remain the same for all core fold patterns. The variations
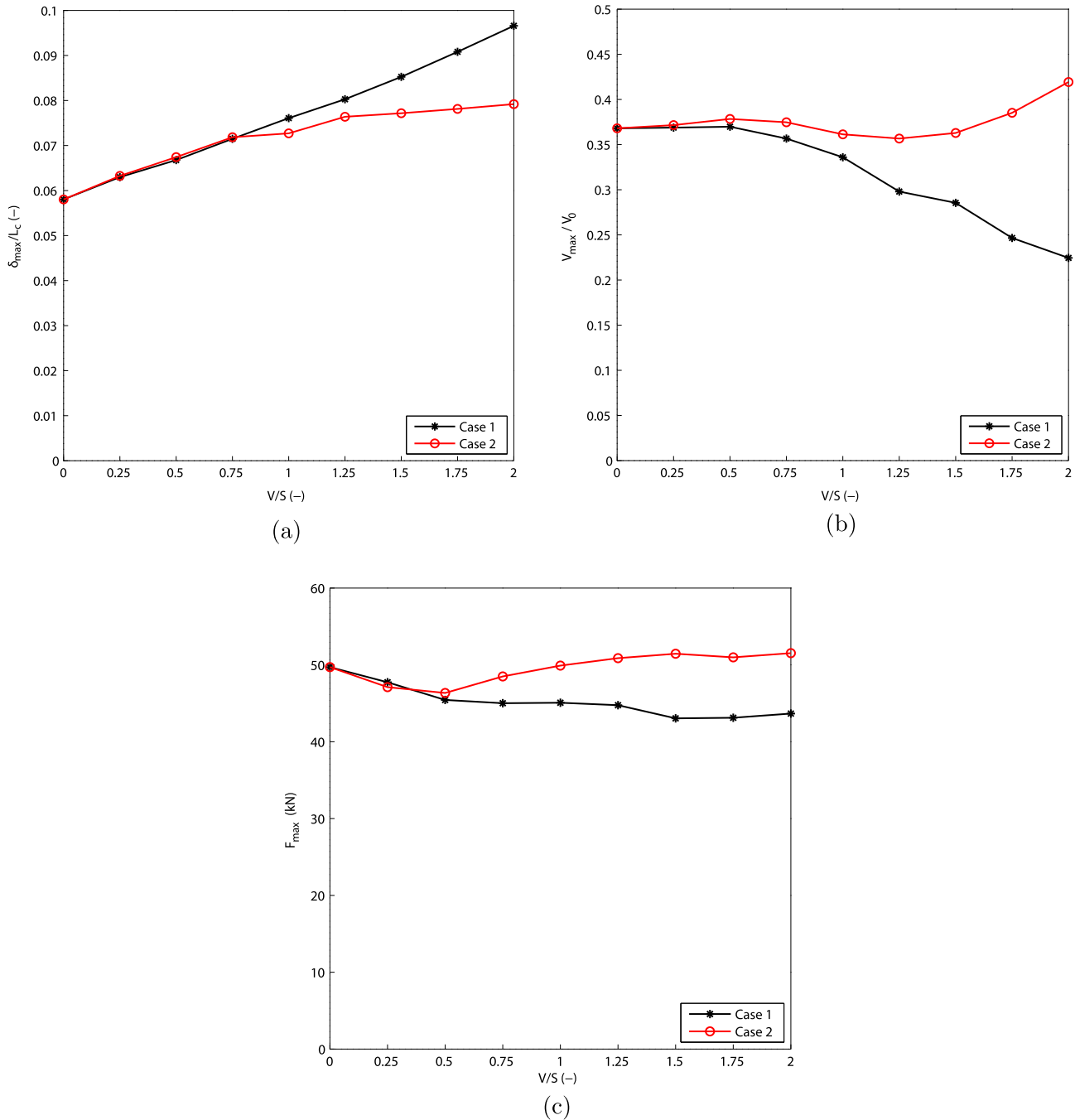
**Fig. 15.** Summary of key performance metrics, for load cases 1 and 2. (a) Maximum back face deflection. (b) Peak back face velocity. (c) Maximum support reaction force.

in sheet thickness will, however, influence the core compressive strength compared to Case 1. Table 2 shows the sheet thicknesses used in the finite element calculations.

### 4.3. Results for Case 1: fixed core sheet thickness t

The dynamic collapse of sandwich beams with increasing values of the fold parameter $V/S$ are shown in Figs. 9–11 for the Case 1 beam configuration. $V/S = 0$ (the prismatic core, Fig. 9), shows the highest apparent core strength. Very little core compression takes place, with core buckling mostly concentrated near to the back face supports. For the intermediate case $V/S = 1$ (Fig. 10) more core compression occurs, concentrated at the moving face sheet (a consequence of the dynamic loading). The core with

$V/S = 2.00$ (Fig. 11) shows the softest core response, with almost complete densification of the core taking place. Subsequently, significant elastic flexure of the beam and core spring back takes place.

The motion of the face sheets is shown in more detail in Figs. 12 and 13, showing the time evolution of the normalised face sheet deflections ($\delta/D_c$) and velocities ($v/v_0$), respectively (both measured at the central node of each face sheet). For all values of $V/S$, three phases of response can be observed. (I) The first is the core compression phase. The front face is decelerated and the back face accelerated until the velocities equalise and core compression ceases. (II) In the second phase the beam bends with little change in core compression, front and back faces moving together, until the beam comes to rest at the point of maximum deflection. (III)
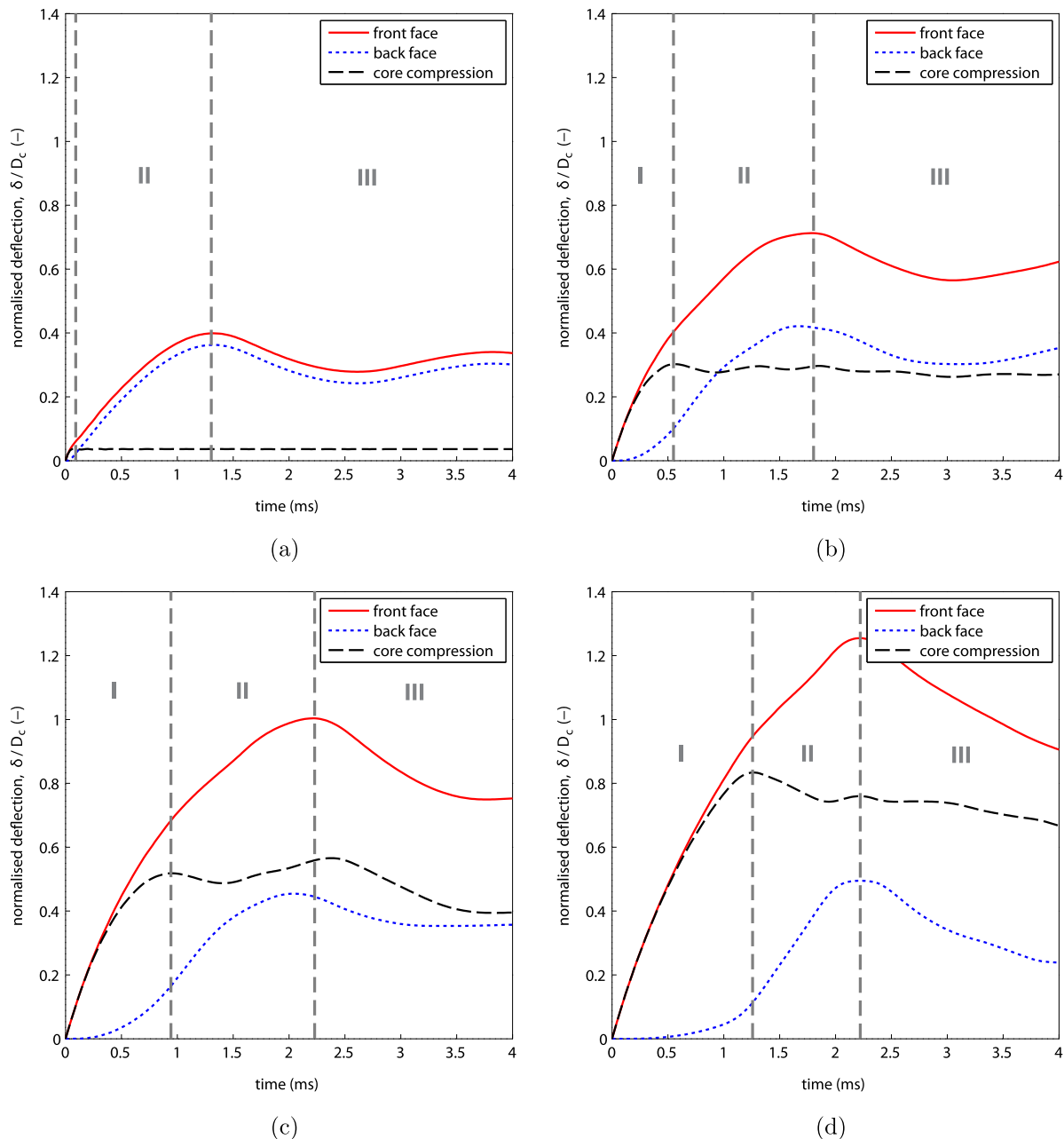
**Fig. 16.** Case 2, deflection $\delta$ at the centre of the front and back face sheets, normalised by the core depth $D_c$. The nominal core compression at mid-span, given by the difference between the normalised face sheet deflections, is also plotted. The three phases of response are indicated. (a) $V/S = 0$, (b) $V/S = 0.5$, (c) $V/S = 1$, (d) $V/S = 2$.

Elastic oscillations then take place in phase three. These response phases have been observed previously for beams with homogeneous foam cores (Fleck and Deshpande, 2004; Tilbrook et al., 2006). The fold parameter $V/S$ of the current core topology influences some key aspects of these response phases:

1. Durations of the phases: Recent theoretical and finite element modelling work (Fleck and Deshpande, 2004; Tilbrook et al., 2006) has shown that the timescales, and overlap, of the phases of sandwich beam response play an important role in blast resistance. From Fig. 12 it can be seen that increasing $V/S$ increases the duration of phase I, the core compression phase. For $V/S = 0$ the velocities of front and back face sheet equalise almost instantaneously, while for $V/S = 2$ phase I lasts for

$\sim 1$ ms. However, the time difference between the end of phase I (core compression) and the end of phase II (beam bending) appears to be insensitive to $V/S$.

2. Back face sheet motion: The face sheet velocities at the point at which they equalise (which is approximately equal to the peak back face sheet velocity) reduces as $V/S$ is increased. However, the maximum beam deflection increases, as a result of the higher core compression in phase I and therefore lower beam bending stiffness in phase II.

3. Elastic recovery in phase III: For large $V/S$, elastic spring back results in the core partly recovering after blast loading, i.e. the permanent core compression is significantly less than the maximum. This is relevant for the post impact structural integrity of the sandwich panel.
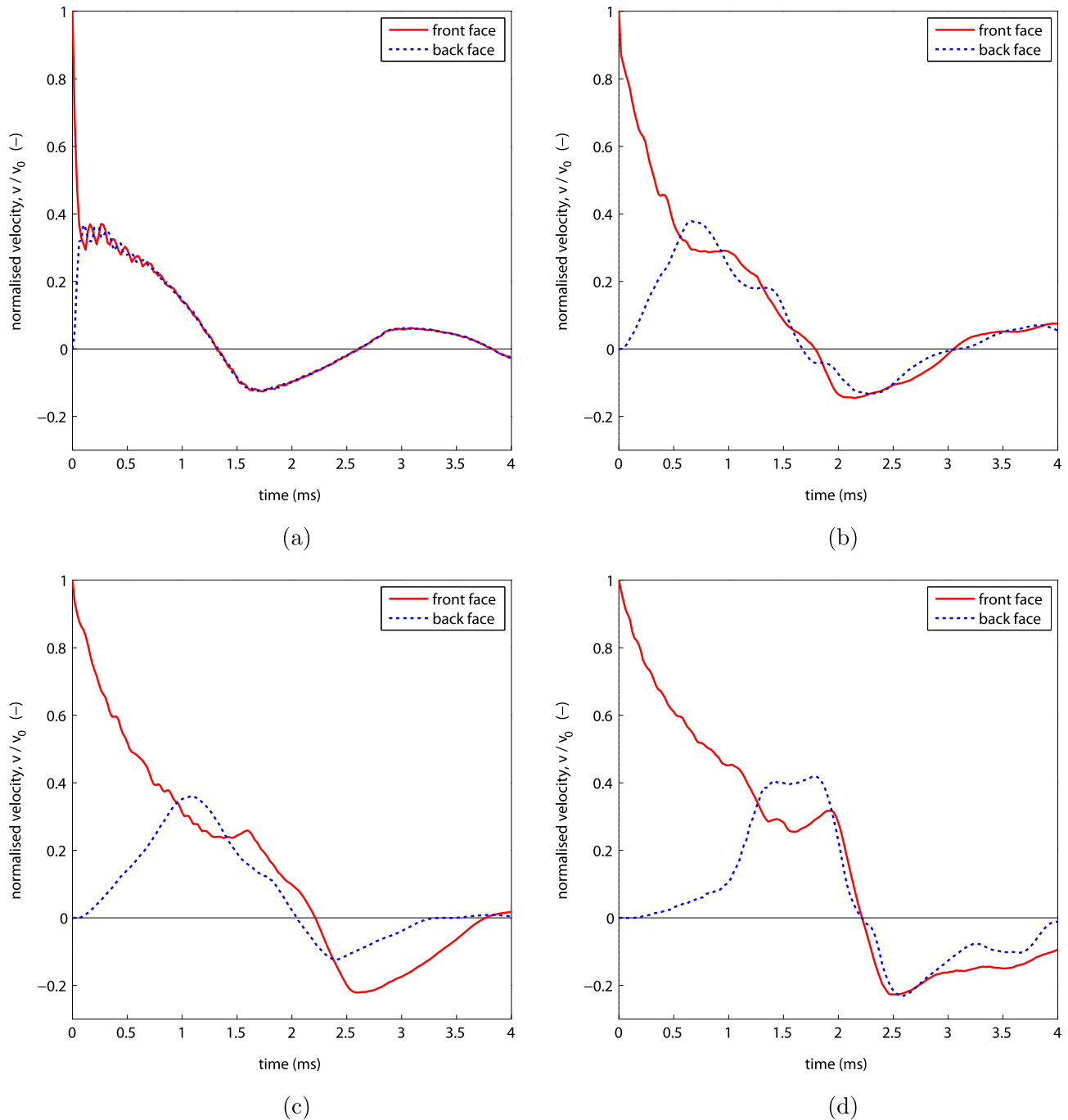
**Fig. 17.** Case 2, velocity $v$ at the centre of the front and back face sheets, normalised by the initial front face velocity $v_0$. (a) $V/S = 0$, (b) $V/S = 0.5$, (c) $V/S = 1$, (d) $V/S = 2$.

The time variation in the reaction forces at the back face sheet supports are shown in Fig. 14 for four values of fold parameter $V/S$. Increasing $V/S$ significantly reduces the reaction force during the core compression phase. However, the peak reaction force, coinciding approximately with the end of phase II, is similar in all cases, reducing slightly with increasing $V/S$. Note that the reaction forces are not equal at both ends of the beam, due to the asymmetry of the core. This becomes more pronounced for increasing $V/S$.

A summary of the key performance metrics maximum back face deflection, maximum back face velocity and maximum support reaction force, and their dependence on the fold parameter $V/S$, is shown in Fig. 15. For Case 1, each performance metric changes monotonically with increasing $V/S$, peak deflection increasing and peak velocity and reaction force decreasing. However, recall that for Case 1 the imparted kinetic energy increases with increasing fold parameter $V/S$ due to the reduction in the front face sheet mass. The influence of this will be considered in Case 2, next.

### 4.4. Results for Case 2: fixed face sheet thickness $t_f$

The results of the Case 2 finite element calculations are presented in Figs. 16–18. The key performance metrics are included in Fig. 15. While the results match Case 1 for low $V/S$, at high $V/S$ maximum back face velocity and support reaction forces are both higher than for Case 1. This is because the lower core strength compared to Case 1 (due to the smaller sheet thickness $t$) means that at high $V/S$ the face sheets still have a significant velocity difference when the core densifies, and 'slap' together (a regime noted
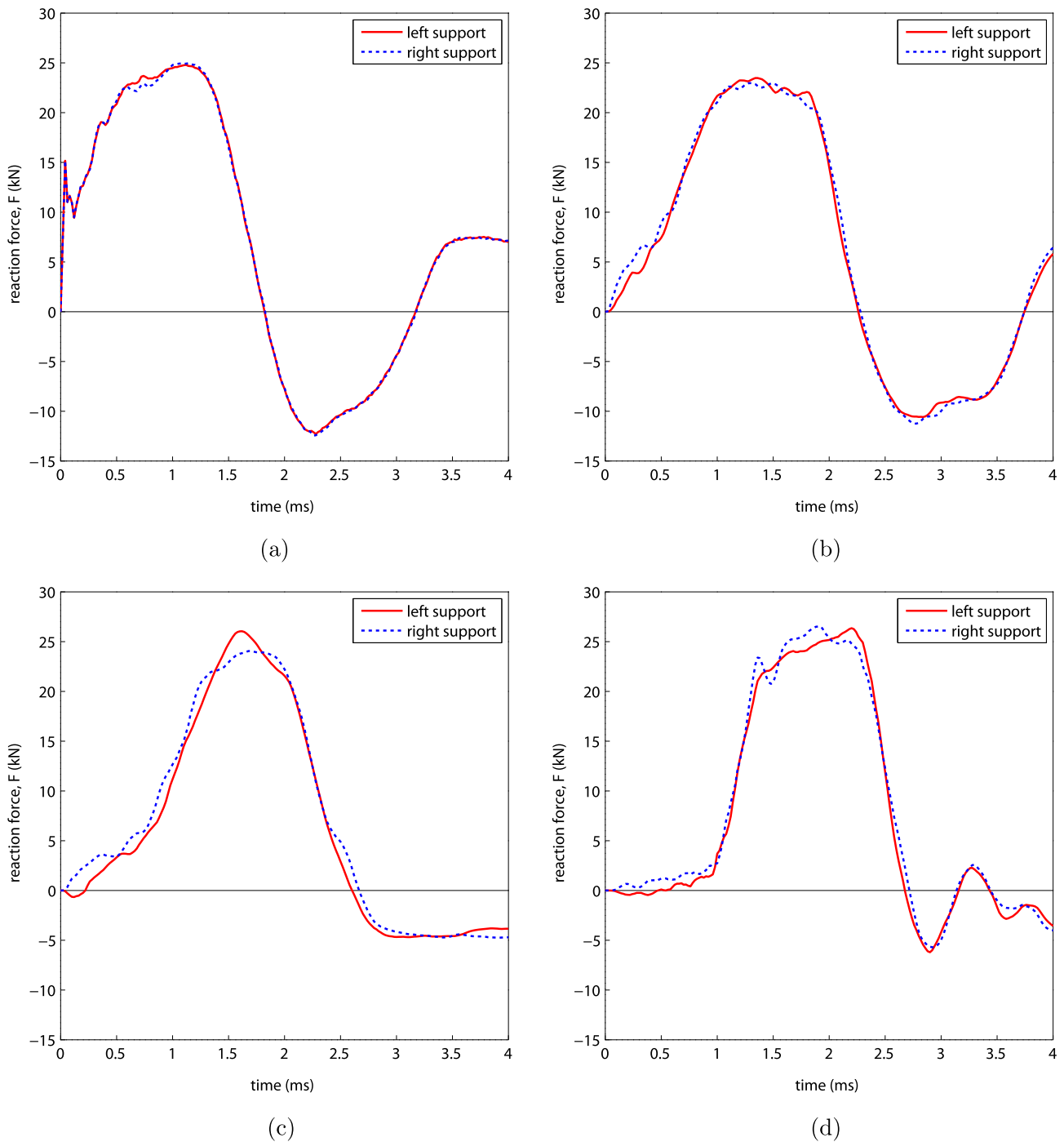
**Fig. 18.** Case 2, vertical reaction forces at the supports. (a) $V/S = 0$, (b) $V/S = 0.5$, (c) $V/S = 1$, (d) $V/S = 2$.

by Tilbrook et al. (2006) for low strength foam cores). This can be seen most clearly in Fig. 17(d). The deformation sequence in Fig. 19 also shows the very soft core responses seen for larger $V/S$. Note that core densification occurs first at the beam supports, and the core compression in the centre of the beam (plotted in Fig. 16) is lower. Unlike many core topologies, the fold pattern of the stacked folded core can be graded continuously through the core thickness. This feature could be used to optimise the core properties, to take advantage of the best aspects of both soft and strong core characteristics.

### 4.5. Comment on model refinement

A characteristic of the stacked folded cellular material is that the global core mechanics is strongly dependent on local effects, in particular (i) the developing plastic hinges at the fold lines, and (ii) the interfaces between stacked folded sheets (here taken to be perfectly bonded). In this preliminary study, our focus has been on establishing the global core response, rather than the detailed behaviour at these fold lines. It is noted however that locally high plastic strains are observed along the hinge lines
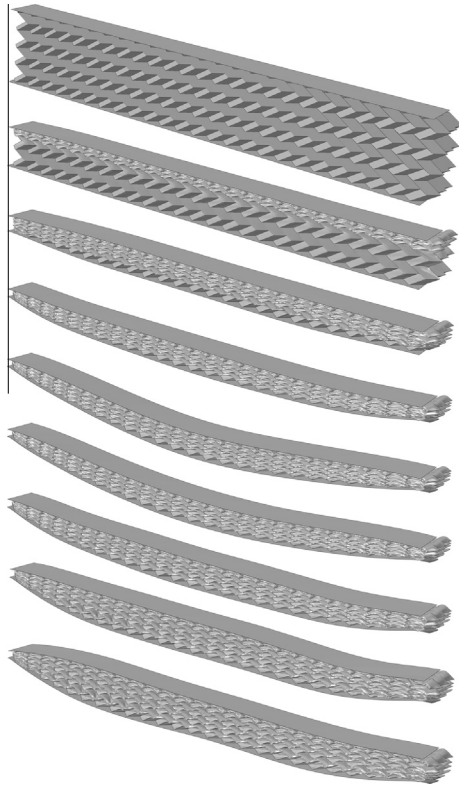
**Fig. 19.** Case 2, deformation of the beam with $V/S = 1.5$; snapshots taken at 0.5 ms intervals.

during the finite element calculations of the compressive collapse of the core. In some places along the hinge lines the plastic strain reaches unrealistically large levels, in excess of the failure strain of the material. Further investigation will be required to examine, for example, the development of damage at the folds, and the implications of this for energy absorption. The choice of constitutive model governing plastic deformation of the hinge lines will also require further investigation, to understand its influence on, for example, compressive strength and elastic spring back of the core. Further detailed analysis is also required of the interfaces between the stacked layers, as interfacial damage along the

common fold lines may also be important. For all calculations reported here, the face sheet equivalent plastic strain never exceeds 0.14, and so omitting face sheet failure is reasonable for this material and loading combination. However, face sheet damage may need to be accounted for at higher blast impulses.

## 5. Conclusions

We have presented a novel cellular material constructed from a stack of folded sheets employing the *Miura* fold pattern. The concept deploys the *Miura* sheets with a unique stacking arrangement and orientation that allows the compressive collapse of the cellular material to be altered through the fold pattern of the layers. The core geometry has an exceptionally wide range of free parameters, which in turn gives unique flexibility to tailor the mechanical properties of the core. We have considered the application of this material as the core of a sandwich beam, and have used finite element analysis to assess its response to quasi-static out-of-plane compression and simulated blast loading. The current investigation is the first assessment of this core structure and its suitability to these applications. The following conclusions are made:

1. By adjusting one fold parameter, the 'chevron' angle characterised by $V/S$, the quasi-static compressive strength of the core can be varied over a wide range. Two modes of collapse have been identified. For $V/S \lesssim 1$, the core achieves a high peak strength, but undergoes subsequent strong softening, due to the localisation of deformation within the core. For $V/S \gtrsim 1$, the core undergoes more uniform collapse, deforming with approximately constant compressive strength.
2. The onset of localised deformation within the core, particularly at small $V/S$, has been shown to depend on the boundary constraints. Increasing the number of cells in the stack reduces the tendency for localisation of collapse.
3. When subjected to impulsive loading, representative of a blast, a wide range of sandwich beam behaviours were achieved by altering the fold parameter $V/S$, from a strong core response with minimal core compression to a very soft response in which full core collapse and densification occured. In addition to core compression, the duration of the core compression phase, peak beam deflection and the reaction forces transmitted to the supports were also influenced. By adjusting either the face sheet thickness or folded sheet thickness in tandem with $V/S$, this
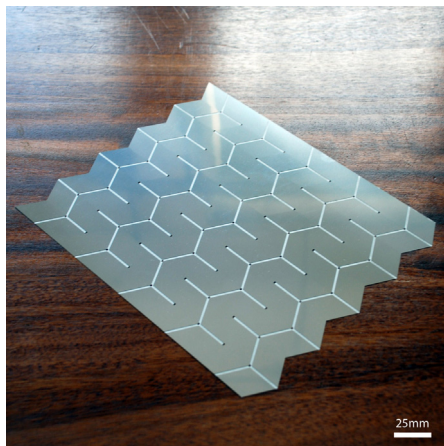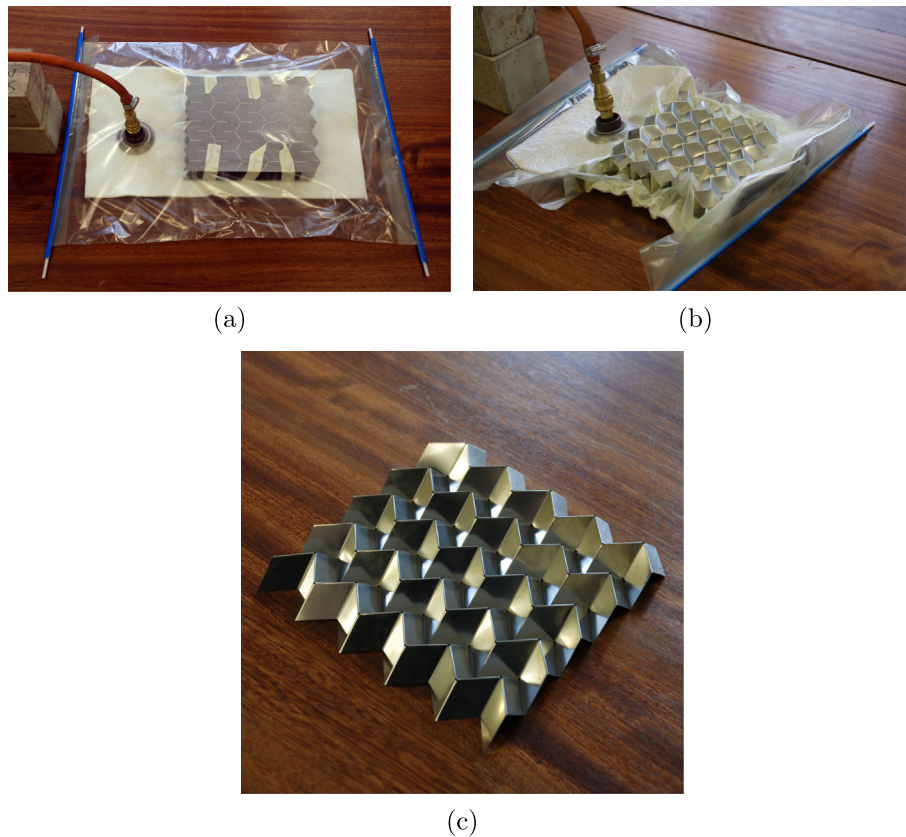


(a)
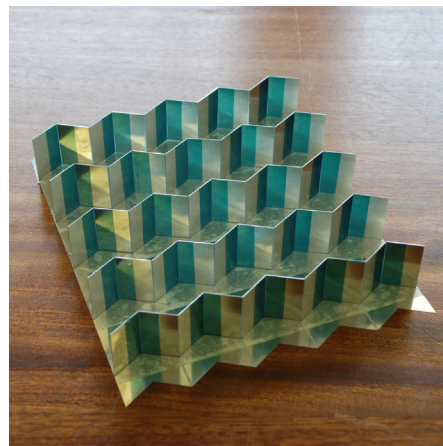


(b)

**Fig. A1.** (a) The fold pattern half-etched into 0.2 mm stainless steel sheet, with mountain and valley folds are etched on opposite sides. (b) Freely hinging spacer plates are positioned along the etched fold lines of the sheet, before an identical etched sheet is placed on top.

**Fig. A2.** The folding process: (a) a sandwich of two etched sheets separated by spacer plates are placed inside a vacuum bag; (b) as the air is removed, the sheets fold along all fold lines simultaneously; (c) the final folded sheet.

range of responses can be achieved without altering the beam mass. This versatility can be used to optimise the sandwich response to particular threats.

4. For most values of chevron angle $V/S$ considered in this study, the compressive collapse strength of the stacked folded core is comparable (for a similar relative density and cell wall material) to other bending dominated cellular materials, such as foams and honeycombs. However, the rich design space of the core offers unique scope for optimisation. The collapse kinematics offers distinct mechanical properties, including auxetic behaviour, tunable through the fold pattern. It is possible to grade the core properties by adjusting the fold parameters continuously through the stack. Manufacturing techniques have also been established for the continuous and efficient production of the folded *Miura* sheet from which the core is constructed.

**Acknowledgements**

**Appendix A. Prototype manufacturing process**

Here we describe a process for manufacturing prototype metal-lic folded plates suited to laboratory scale investigations of the stacked folded core. The folding method is based on that developed by Schenk et al. (2011), and is a synchronous folding method which requires minimal tooling, and is therefore well-suited for prototyping purposes. To assist folding, the sheets are first locally weakened along the fold lines. This can be achieved by locally thinning the material along the fold lines by chemical etching. Fig. A1(a) shows a stainless steel sheet (0.2 mm thickness) with the fold pattern (3 mm wide fold lines) etched through half of the sheet thickness. The 'mountain' and 'valley' folds were etched on opposite sides of the sheet; as a result, where the fold lines on opposite sides meet at the vertices, the material was completely removed. This is desirable, in order to avoid complex material deformations at the vertices. Next, a series of freely hinged spacers (consisting of metal plates joined together with adhesive tape to provide the hinge) are placed along the fold lines of the etched plate: see Fig. A1(b). A second identically etched plate is placed on top of the spacers, parallel with the first sheet. The combination is packed into an air-tight bag, which is connected to a vacuum pump. As the air is removed the resulting pressure difference bends the material along the fold lines; see Fig. A2(a and b). The biaxial contraction during the folding process is enabled by the freely hinging spacers. The fold depth is limited by the eventual contact between the two sheets, which is determined by the height of the spacers. A resulting folded sheet is shown in Fig. A2(c). The manufacturing process produced an accurately folded sheet with no material deformation other than bending along the fold lines.

**References**

Akishev, N.I., Zakirov, I.M., Nikitin, A.V., 2009. Device for sheet material corrugation. US Patent 7487658.

Baranger, E., Guidault, P.A., Cluzel, C., 2011. Numerical modeling of the geometrical defects of an origami-like sandwich core. Compos. Struct. 93, 2504–2510. http://dx.doi.org/10.1016/j.compstruct.2011.04.011.

Basily, B., Elsayed, E., 2004. Dynamic axial crushing of multilayer core structures of folded chevron patterns. Int. J. Mater. Prod. Technol. 21, 169–185. http://dx.doi.org/10.1504/IJMPT.2004.004750.

Côté, F., Deshpande, V., Fleck, N., Evans, A., 2004. The out-of-plane compressive behavior of metallic honeycombs. Mater. Sci. Eng.: A 380, 272–280. http://dx.doi.org/10.1016/j.msea.2004.03.051.

Côté, F., Deshpande, V., Fleck, N., Evans, A., 2006. The compressive and shear responses of corrugated and diamond lattice materials. Int. J. Solids Struct. 43, 6220–6242. http://dx.doi.org/10.1016/j.ijsolstr.2005.07.045.

Deshpande, V., Fleck, N., 2000. High strain rate compressive behaviour of aluminium alloy foams. Int. J. Impact Eng. 24, 277–298. http://dx.doi.org/10.1016/S0734-743X(99)00153-0.

Doyoyo, M., Mohr, D., 2003. Microstructural response of aluminum honeycomb to combined out-of-plane loading. Mech. Mater. 35, 865–876.

Elsayed, E.A., Basily, B., 2004. A continuous folding process for sheet materials. Int. J. Mater. Prod. Technol. 21, 217–238. http://dx.doi.org/10.1504/IJMPT.2004.004753.

Fleck, N., Deshpande, V., 2004. The resistance of clamped sandwich beams to shock loading. J. Appl. Mech. 71, 386–401. http://dx.doi.org/10.1115/1.1629109.

Gibson, L.J., Ashby, M.F., 1999. Cellular Solids, Second ed. Cambridge University Press.

Heimbs, S., 2009. Virtual testing of sandwich core structures using dynamic finite element simulations. Comput. Mater. Sci. 45, 205–216. http://dx.doi.org/10.1016/j.commatsci.2008.09.017.

Heimbs, S., Cichosz, J., Klaus, M., Kilchert, S., Johnson, A., 2010. Sandwich structures with textile-reinforced composite foldcores under impact loads. Compos. Struct. 92, 1485–1497, <http://dx.doi.org/10.1016/j.compstruct.2009.11.001>.

Hochfeld, H., 1959. Process and machine for pleating pliable structures. US Patent 2901951.

Ichikawa, H., 1995. Method of production of reinforced composite corrugated body and method of formation of corrugating rollers for use therein. US Patent 5443779.

Johnson, G.R., Cook, W.H., 1983. A constitutive model and data for metals subjected to large strains, high strain rates and high temperatures. In: Proceedings of the 7th International Symposium on Ballistics, The Hague, The Netherlands. pp. 541–547.

Kehrle, R., 2005. Method and apparatus for producing a composite structural panel with a folded material core. US Patent 6913570.

Khaliulin, V.I., 2005. A technique for synthesizing the structures of folded cores of sandwich panels. Russ. Aeronaut. (Iz VUZ) 48, 7–12.

Khaliulin, V.I., Batrakov, V.V., Dvoeglazov, I., Menjashkin, D.G., 2007. Method for making parts with zigzag corrugated structure. Russian Patent RU2303501.

Khaliulin, V.I., Dvoeglazov, I.V., 2001. On technological problems of fabrication of relief designs by isometric transformation of thin sheet. Trans. Nanjing Univ. Aeronaut. Astronaut. 18, 11–16.

Klett, Y., Drechsler, K., 2010. Designing technical tessellations. In: Wang-Iverson, P., Lang, R.J., YIM, M. (Eds.), Origami 5: Fifth International Meeting of Origami Science, Mathematics, and Education (5OSME). CRC Press, pp. 305–322. http://dx.doi.org/10.1201/b10971-28.

Kling, D., 2007. Folding method and apparatus. US Patent Application 20070273077.

Kling, D., 2010. Folding methods, structures and apparatuses. US Patent Application 20100006210.

Kooistra, G., Deshpande, V., Wadley, H., 2004. Compressive behavior of age hardenable tetrahedral lattice truss structures made from aluminium. Acta Mater. 52, 4229–4237. http://dx.doi.org/10.1016/j.actamat.2004.05.039.

Lakes, R., 1987. Foam structures with a negative poisson's ratio. Science 235, 1038–1040. http://dx.doi.org/10.1126/science.235.4792.1038.

Lebée, A., Sab, K., 2010. Transverse shear stiffness of a chevron folded core used in sandwich construction. Int. J. Solids Struct. 47, 2620–2629. http://dx.doi.org/10.1016/j.ijsolstr.2010.05.024.

Liang, Y., Spuskanyuk, A., Flores, S., Hayhurst, D., Hutchinson, J., McMeeking, R., Evans, A., 2007. The response of metallic sandwich panels to water blast. J. Appl. Mech. 74, 81–99. http://dx.doi.org/10.1115/1.2178837.

McShane, G., Deshpande, V., Fleck, N., 2007. The underwater blast resistance of metallic sandwich beams with prismatic lattice cores. J. Appl. Mech. 74, 352–364. http://dx.doi.org/10.1115/1.2198549.

McShane, G., Pingle, S., Deshpande, V., Fleck, N., 2012. Dynamic buckling of an inclined strut. Int. J. Solids Struct. 49, 2830–2838. http://dx.doi.org/10.1016/j.ijsolstr.2012.03.045.

Miura, K., 1972. Zeta-core sandwich-its concept and realization. ISAS Report 37, 137–164. Institute of Space and Aeronautical Science, University of Tokyo report, no 480. <http://ci.nii.ac.jp/naid/110001101664>

Miura, K., 2006. The science of miura-ori: a review. In: R.J., Lang (Eds.), Origami 4: Fourth International Meeting of Origami Science, Mathematics, and Education (4OSME). AK Peters, p. 8799. http://dx.doi.org/10.1201/b10653-12.

Mohr, D., Doyoyo, M., 2004. Experimental investigation on the plasticity of hexagonal aluminum honeycomb under multiaxial loading. J. Appl. Mech. Trans. ASME 71, 375–385.

Nemat-Nasser, S., Guo, W.G., 2005. Thermomechanical response of hsla-65 steel plates: experiments and modeling. Mech. Mater. 37, 379–405. http://dx.doi.org/10.1016/j.mechmat.2003.08.017.

Radford, D., McShane, G., Deshpande, V., Fleck, N., 2006. The response of clamped sandwich plates with metallic foam cores to simulated blast loading. Int. J. Solids Struct. 43, 2243–2259. http://dx.doi.org/10.1016/j.ijsolstr.2005.07.006.

Radford, D., McShane, G., Deshpande, V., Fleck, N., 2007. Dynamic compressive response of stainless-steel square honeycombs. J. Appl. Mech. 74, 658–667. http://dx.doi.org/10.1115/1.2424717.

Rapp, E.G., 1960. Sandwich-type structural element. US Patent 2963128.

Schenk, M., 2011. Folded shell structures (Ph.D. thesis). University of Cambridge.

Schenk, M., Allwood, J.M., Guest, S.D., 2011. Cold gas-pressure folding of miura-ori sheets. In: International Conference on Technology of Plasticity (ICTP 2011), Aachen, Germany.

Schenk, M., Guest, S.D., 2013. Geometry of miura-folded meta-materials. Proc. Natl. Acad. Sci. (PNAS) 110, 3276–3281, <http://dx.doi.org/10.1073/pnas.1217998110>.

Sypeck, D., Wadley, H., 2001. Multifunctional microtruss laminates: textile synthesis and properties. J. Mater. Res. 16, 890–897. http://dx.doi.org/10.1557/JMR.2001.0117.

Tilbrook, M.T., Deshpande, V.S., Fleck, N.A., 2006. The impulsive response of sandwich beams: analytical and numerical investigation of regimes of behaviour. J. Mech. Phys. Solids 54, 2242–2280. http://dx.doi.org/10.1016/j.jmps.2006.07.001.

Vaughn, D., Hutchinson, J., 2006. Bucklewaves. Eur. J. Mech. – A/Solids 25, 1–12. http://dx.doi.org/10.1016/j.euromechsol.2005.09.003.

Xue, Z., Hutchinson, J., 2004. A comparative study of impulse-resistant metal sandwich plates. Int. J. Impact Eng. 30, 1283–1305. http://dx.doi.org/10.1016/j.ijimpeng.2003.08.007.